Review article

In vivo bioprinting: Broadening the therapeutic horizon for tissue injuries

Wenxiang Zhao [a,b], Chuxiong Hu [a,b,*], Tao Xu [c]

[a] *State Key Laboratory of Tribology, Department of Mechanical Engineering, Tsinghua University, Beijing, 100084, China*
[b] *Beijing Key Laboratory of Precision/Ultra-Precision Manufacturing Equipments and Control, Tsinghua University, Beijing, 100084, China*
[c] *Center for Bio-intelligent Manufacturing and Living Matter Bioprinting, Research Institute of Tsinghua University in Shenzhen, Tsinghua University, Shenzhen, 518057, China*

ARTICLE INFO

ABSTRACT

Tissue injury is a collective term for various disorders associated with organs and tissues induced by extrinsic or intrinsic factors, which significantly concerns human health. *In vivo* bioprinting, an emerging tissue engineering approach, allows for the direct deposition of bioink into the defect sites inside the patient's body, effectively addressing the challenges associated with the fabrication and implantation of irregularly shaped scaffolds and enabling the rapid on-site management of tissue injuries. This strategy complements operative therapy as well as pharmacotherapy, and broadens the therapeutic horizon for tissue injuries. The implementation of *in vivo* bioprinting requires targeted investigations in printing modalities, bioinks, and devices to accommodate the unique intracorporal microenvironment, as well as effective integrations with intraoperative procedures to facilitate its clinical application. In this review, we summarize the developments of *in vivo* bioprinting from three perspectives: modalities and bioinks, devices, and clinical integrations, and further discuss the current challenges and potential improvements in the future.

1. Introduction

Tissue injury, defined as the loss or failure of organs and tissues due to unanticipated trauma, surgical complications, or ageing, is one of the significant causes for concerns in human health care [1]. Tissue injury is a collective term for many disorders and encompasses a broad spectrum. Among them, extensive skin injuries, volumetric muscle loss (VML), and bone defects induced by mechanical factors, heat, and other unintended external causes are the most common types of tissue injury disorders [2,3]. As for surgical complications, additional injuries might be caused by surgical operations [4]. In the case of intracranial aneurysm treatment, for instance, the removal of the interventional removal of the aneurysm inevitably leads to a breach in the vessel wall and consequent histological damage [5]. Ageing leads to various physiological, metabolic, and functional changes in the human body, such as peptic ulcers [6,7] and endometrial thinning [8], which also account for a certain proportion of tissue injury and have various degrees of impact on human health.

The clinical requirements for tissue injury repair include (i) rapid treatment and healing to prevent fluid loss or infection. (ii) minimally invasive to reduce the postoperative recovery period and the risk of complications. (iii) personalization and (iv) functionality, aiming to provide the repaired tissues with appropriate physiological properties resembling the native tissues.

The current options for tissue injury repair can be broadly summarized as operative therapy, pharmacotherapy, etc. Among these, operative therapy, with operations including excision and suturing to treat the lesions, is well-developed and capable of most tissue injury diseases [9–11]. However, limitations still exist, including the risk of infection associated with open wound exposure, the difficulty when applied to tissues with elasticity and sealing requirements, and uncertainty in therapeutic effects depending on the surgeons [11–13]. Medication can be administered orally or by injection to treat tissue injuries. However, its limited therapeutic pertinence and the potential risk of drug resistance as well as metabolic burden may restrict its long-term use in clinical treatment [14,15].

Bioprinting refers to the fabrication of scaffolds based on the discrete-collecting principle, which incorporates layer-by-layer deposition of bioinks (biomaterial comprising cells) with predefined 3D structures developed in computer-aided design (CAD) software [16].

After decades of development, it has become possible to construct complex 3D tissues and organs by selecting the appropriate biomaterials, cell types, and growth factors, providing an effective solution for filling and repairing tissue injuries [17–19]. The reverse engineering properties of bioprinting and the culture modulation process are essential for the personalized and functional requirements of tissue injury repair, but its intracorporal implementation is still confronted with challenges [20].

The strategy for treating tissue injuries through bioprinting can be abstracted as an "*in vitro* bioprinting and subsequent implantation" approach, and challenges with this approach include (i) the *in vitro* culture of tissues to maturity typically takes several weeks, which tends to cause the miss of optimal period for treatment; (ii) difficulties exist in creating a dynamic and biomimetic artificial microenvironment essential in tissue development; (iii) the risk of impairment or contamination of the constructed tissues due to transportation and manual implantation, and (iv) the potential mismatch between tissue scaffolds and injured sites caused by the dynamic intracorporeal environment and the

resolution limit of *in vitro* imaging devices. Therefore, there is a need for a new paradigm utilizing bioprinting techniques in tissue injury repair.

In vivo bioprinting (also referred to as *in situ* bioprinting, intraoperative bioprinting, or intravital bioprinting) is a promising strategy for the above challenges. It is defined as the direct printing of bioinks inside the defect to create or repair living tissues in a clinical setting [21] (Fig. 1). It has developed rapidly in the skin, bone, and cartilage repair [22–25], benefiting from the ideal accessibility or relative simplicity of these tissues.

The primary feature of *in vivo* bioprinting is integrating the two-step "print-implantation" strategy. In the surgical setting, the surface appearance can be acquired with high precision in real-time, which allows the bioprinting process to be adapted according to the changes in the defect microenvironment over time due to the dynamic nature of wounds. Therefore, the printed tissue scaffold accurately matches the defect geometry. In addition, the adhesion of the scaffold to the residual tissues is enhanced via *in situ* crosslinking, enabling stable tissue-scaffold integration and eliminating the risk of contamination and disruption of
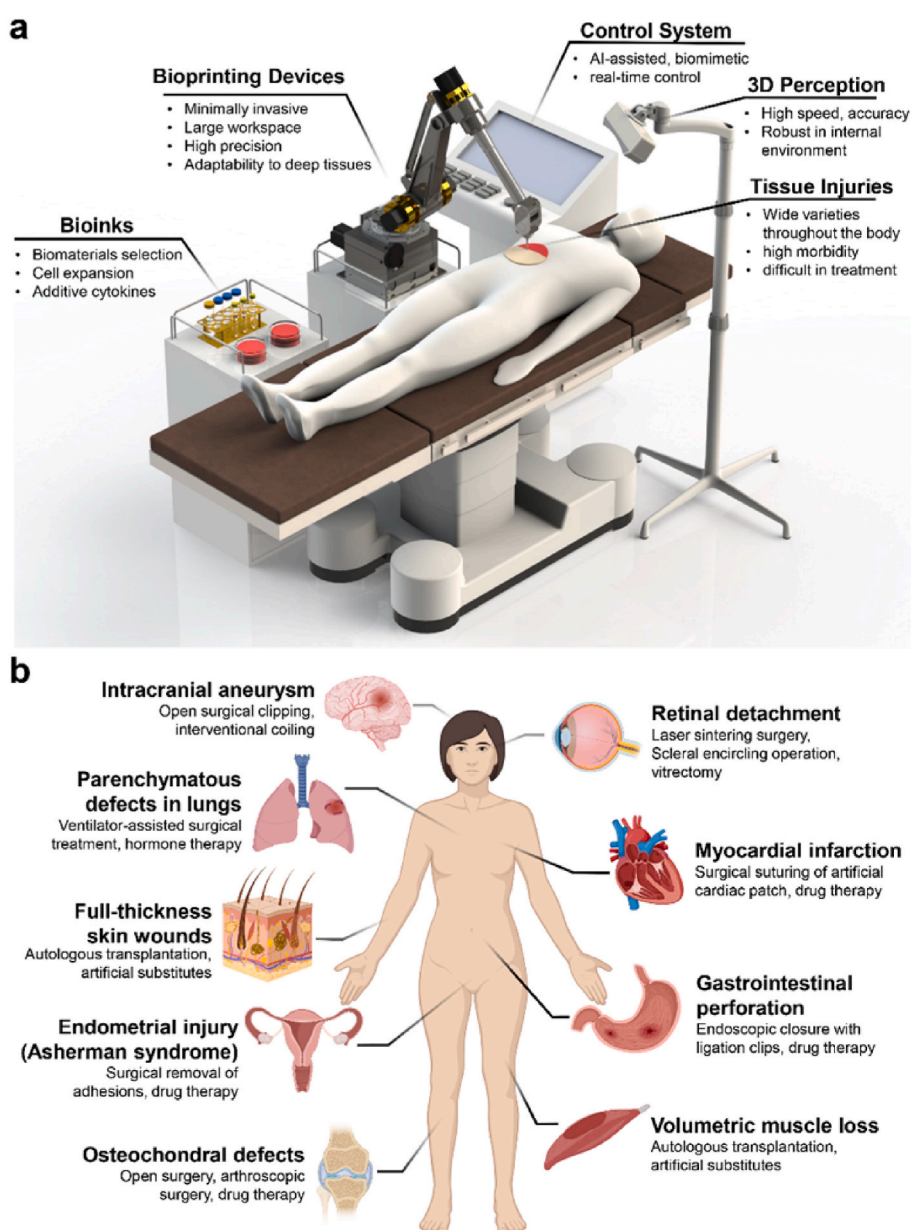

Fig. 1. a, Schematic diagram of the clinical implementation of *in vivo* bioprinting for tissue injuries repair. **b,** Typical tissue injuries in humans, spreading throughout the body. Fig. 1b is created with Biorender.com.

the fragile hydrogel-based tissue scaffold during transplantation and suturing. Secondly, *in vivo* bioprinting creates an ideal condition for the tissue scaffold using the host's native microenvironment. This natural bioreactor provides the appropriate nutrients and dynamic stimulations for tissue development, facilitating cells' proliferation, migration, and integration within the scaffold and native tissues. This rapid *in situ* fill-in treatment prevents patients from waiting for mature tissues long-term and dramatically improves the efficiency of tissue injury repair. With the personalized and built-from-scratch characters, the tissue deficiency diseases, such as tissue losses or functional failures listed in Fig. 1b can all be intervened and therapied through the concept of *in vivo* bioprinting.

Despite promising, *in vivo* bioprinting is an emerging field that requires advances in technologies, materials, and equipment that differ from conventional bioprinting. This review presents typical developments of *in vivo* bioprinting in terms of methodologies, bioinks,

printing devices, and integration with clinical procedures. We then discuss the possible future trends associated with bioink properties, artificial intelligence technology, and robotics. In the end, we highlight this technology's challenges and potential opportunities.

1.1. Bioprinting modalities and bioinks

Research into bioprinting modalities and bioinks is to pursue how *in vivo* bioprinting can be addressed in the unique intracorporal environment. The primary need for printing treatment on the defect site is the bioinks' one-step crosslinking, which refers to the gelation of bioinks on the spot by only one crosslinking method such as photo-crosslinking, enzymatic crosslinking, ionic crosslinking, etc. Taking alginate-gelatin hydrogel, the popular bioink system in bioprinting research [26], as an example, its application requires temperature control to improve printability and subsequent solidification through secondary
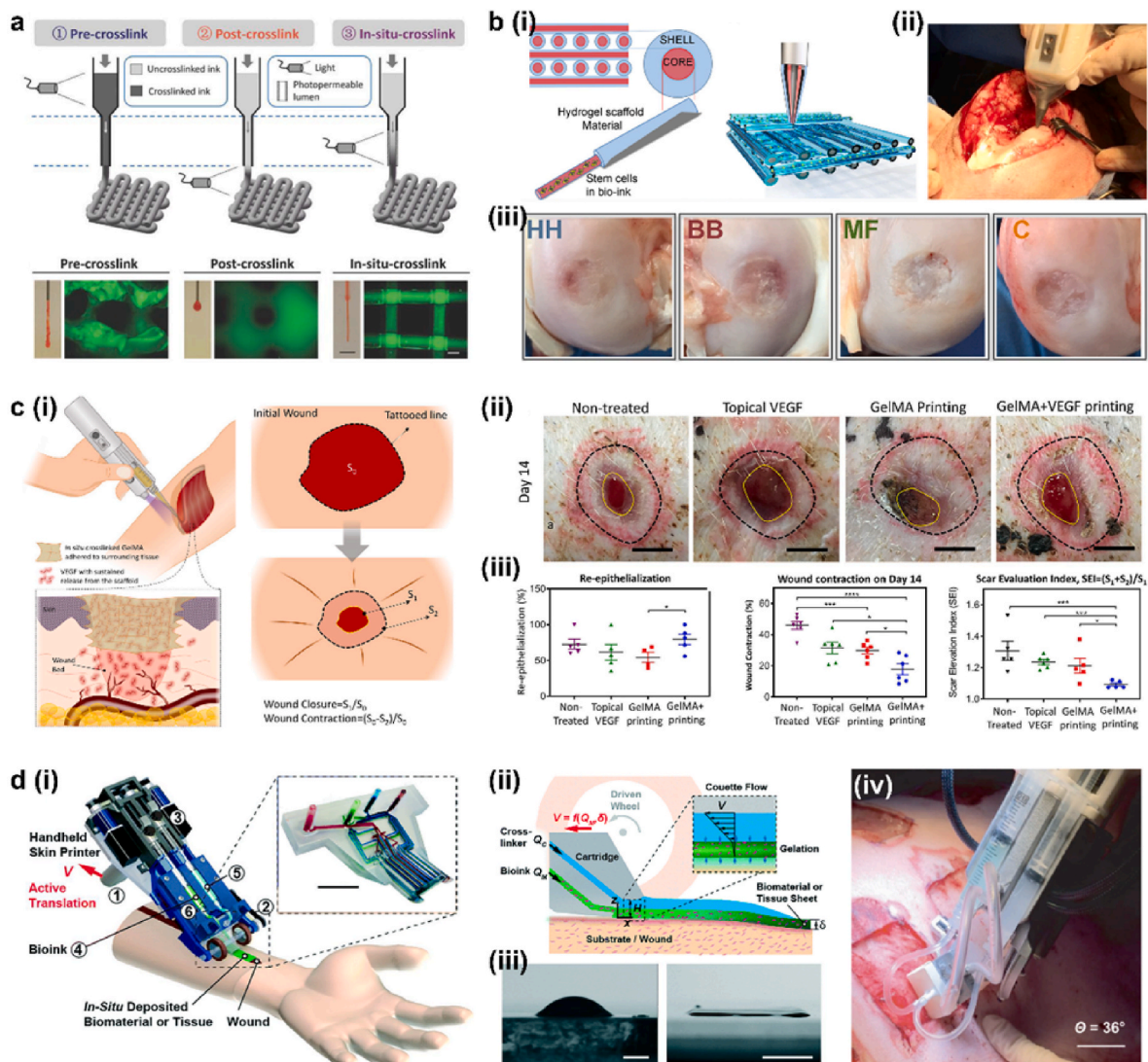

Fig. 2. a, In-situ-crosslink constructs uniform hydrogel filaments with better fidelity than pre-crosslink and post-crosslink, adapted, with permission from Ref. [36]. **b,** Extrusion-based *in situ* bioprinting constructs the Shell-core hydrogel filaments for the treatment of cartilage injuries. (i) Shell-Core structure. (ii) *in situ* bioprinting on the knee. (iii) cartilage defects repaired by *in vivo* bioprinting present better therapeutic results, adapted, with permission from Ref. [40]. (HH: Handheld bioprinting, BB: bench-based bioprinting, MF: microfractures, C: control) **c,** *in vivo* bioprinting of GelMA and VEGF to repair extensive skin trauma. (i) schematic diagram. (ii) representative photographs (Scale bar: 1 cm) and (iii) statistics of the effectiveness of different treatment methods, adapted from Ref. [41], CC BY 4.0. **d,** Extrusion-based microfluidic bioprinting. (i) diagram of the printing device and microfluidic channels. (ii) Schematic diagram and (iii) photographs of the microfluidic channel that prints two components of bioink into a uniform biosheet (Scale bars: 2 mm (left), 5 mm (right)), adapted, with permission from Ref. [51]. (iv) *in situ* implementation of the enzymatic crosslinking bioprinting for the treatment of full-thickness skin wounds in porcine (Scale bar: 2.5 cm), adapted, with permission from Ref. [52].

crosslinking of calcium ions [27]. Although favorable fidelity and biological properties have been achieved in *ex vivo* studies [28–30], this two-step crosslinking is inappropriate for *in vivo* bioprinting due to the incompatibility between the desired temperature and body temperature, extended gelation period and the introduction of calcium ions, an abiotic element with potential toxicity [31].

1.2. Extrusion-based bioprinting

Current *in vivo* bioprinting modalities can be divided into three main categories: extrusion-based bioprinting, stereolithography-based bioprinting, and droplet-based bioprinting. In extrusion-based bioprinting, the bioink responds promptly to a specific stimulation applied to the extrusion nozzle and presents as a continuous and smooth filament suitable for extrusion macroscopically and capable of supporting its weight [32]. Such filaments are deposited layer-by-layer onto the defect site, enabling the construction of a 3D structure. Among them, the photo-responsive extrusion-based bioprinting method has received the majority of attention [33,34]. Combined with a specific wavelength of light and photoinitiators, it enables the stable covalent crosslinking of photosensitive bioinks represented by Methacrylate Gelatin (GelMA) to achieve an irreversible transition from sol to gel [35]. Ouyang et al. pioneered a systematic exploration of *in situ* crosslinking strategy based on photosensitive hydrogels [36] by exploring parameters in terms of light and printing velocity to enable simultaneous extrusion and crosslinking of GelMA. Compared with pre-crosslink and post-crosslink, the *in situ* crosslink strategy effectively enhances the fidelity of the extruded filaments and guarantees lower shear stress within the nozzle, thus safeguarding favorable cell viability (Fig. 2a). In addition, this strategy can be extended to various photosensitive bioinks such as methacrylate hyaluronic acid (HAMA), poly (ethylene glycol) diacrylate (PEGDA) and norbornene-functionalized HA (NorHA).

Due to the desirable biocompatibility and expansibility [37], it is possible to introduce cells or growth factors into the bioinks for tissue injury treatment. O'Connell et al. constructed coaxial filaments in a core-shell manner based on the extrusion-based bioprinting modality, where core bioink encapsulates the stem cells and shell bioink mixed with GelMA + HAMA to provide mechanical strength upon hardening and protect the core cells from UV radiation [38]. *In vitro* studies presented high viability (>97%) of core stem cells in one-week post-printed structures [25,39]. Moreover, the *in situ* printing for chondral defect repair conducted on sheep's stifle joints has also demonstrated better macroscopic and microscopic characteristics than conventional treatments and exhibited an early formation of hyaline-like cartilage (Fig. 2b) [40]. Likewise, Nuutila and colleagues combined GelMA with vascular endothelial growth factor (VEGF) as bioink. They deposited it directly into the porcine full-thickness skin wounds under exposure to blue-violet light, demonstrating a significant improvement in terms of wound contraction and the quality of wound healing (Fig. 2c) [41]. Other scholars have further progressed toward functional recovery of muscle tissues presented in a murine VML injury model [42–44], showing the superiority of photo-responsive extrusion-based bioprinting for tissue injury repair.

In addition, there have also been some exploratory studies of extrusion-based bioprinting based on enzymatic crosslinking, representative of which is the reactions between fibrinogen and thrombin, which has been widely used in tissue engineering due to its autologous properties [45–47]. Nevertheless, its limitations are the extremely low viscosity of the precursor solutions and the rapid crosslinking reactions [48,49], which can easily lead to uncontrollable crosslinking process, inhomogeneous clumping of gels, and other deficiencies [50]. To overcome the challenges during gelation, Guenther's group proposed a microfluidic-based extrusion system that disperses fibrinogen and thrombin precursor solutions in microfluidic channels to react at the microscale, which effectively avoids the non-uniformity of gelation [51, 52]. Controlled by the microfluidic system, thin flake gels with regular

thickness, width, and composition can be obtained that avoid the impact of surface tension. The physiological structure of the "epidermis-dermis" in skin tissues is replicated with gel sheets containing keratinocytes and fibroblasts. The feasibility of *in situ* deposition of architected bio-sheets onto inclined and compliant wound surfaces was demonstrated on the mouse and porcine skin wounds (Fig. 2d). Due to the two-dimensional lamellar structure of the printed unit, it is prospective for the prompt treatment of extensive skin lesions.

There are other alternatives in extrusion-based *in vivo* bioprinting. For instance, the bioink consisting of chitosan and β-glycerophosphate solutions, which can be gelled stably at the body's temperature after optimizing the concentration [53,54], was combined with nano-hydroxyapatite and plasmid-DNA to promote bone repair through *in situ* bioprinting in mice [55]. Mostafavi et al. printed poly(caprolactone) (PCL), an inert biomaterial with a low melting point, onto the VML injury directly for tissue repair utilizing fused deposition modeling (FDM) [56]. Despite the low melting point, it still reached approximately 70 °C and thus needed to cool down by a water-cooled reservoir before contacting the tissues. As for ionic crosslinking, in order to address the difficulties of secondary crosslinking of alginate and calcium ions, Kim et al. applied coaxial bioprinting to achieve *in situ* gelations of these two components [57], while Hazur took $CaCO_3$ as a source of inert calcium ions [58] to achieve crosslinking with the slow-release of calcium ions. Nevertheless, these approaches still cannot avoid the potential cytotoxicity of calcium ions. As a result, relevant research has remained at the proof-of-concept stage of the feasibility of *in situ* bioprinting, while few have explored further biological applications.

1.3. Stereolithography-based bioprinting

The *in situ* SLA bioprinting involves the pre-injection of bioink precursors into the defect site to form a liquid pool and the selective irradiation to create a 3D construct for intracorporal tissue injury repair. In this technology, the penetration of the excitation light into the tissues is essential to achieve external stimulation with minimal invasiveness, which makes the commonly used UV irradiation inappropriate [59,60]. Recently, the development of photo-initiators sensitive to near-infrared (NIR) light has received attention due to its ability to penetrate soft tissues. In 2020, scholars from Sichuan University and the University of Padova reported their progress in NIR-induced non-invasive *in vivo* bioprinting almost simultaneously in different approaches. Chen et al. developed a nanoparticle-mediated photo-initiator to realize the gelation of GelMA under digital micromirror device (DMD) projection [61]. Subcutaneously printed hydrogel structures in different shapes were reported with high cellular viability and proper tissue integration, revealing a therapeutic potential for VML repair (Fig. 3a). Elvassor's team left the photo-initiator behind and presented the two-photon excitation of coumarin derivates for *in vivo* bioprinting [62]. In particular, the multi-photon microscope provides real-time imaging while laser-scanning, constituting a closed-loop bioprinting that achieved resolution at the micron-level (Fig. 3b). Minimally invasive *in situ* SLA bioprinting was successfully implemented for the formation of complex structures inside murine skin, muscle, and brain without adverse effects on neighboring healthy tissues owing to the controlled power. Although it presents advantages, including less invasiveness and high resolution, *in situ* SLA-based bioprinting is limited to the dimensions and depth of printing. Furthermore, it is only suitable for single-component photo-crosslinkable bioinks, and excessive materials injection may lead to material redundancy in areas that are not selectively illuminated.

1.4. Droplet-based bioprinting

The droplet-based *in situ* bioprinting method refers to the deposition of bioink in the droplet form at a predefined location with precise noncontact positioning [63]. The droplets are generated at picolitre scale by thermal, piezoelectric, or laser-assisted methods and therefore
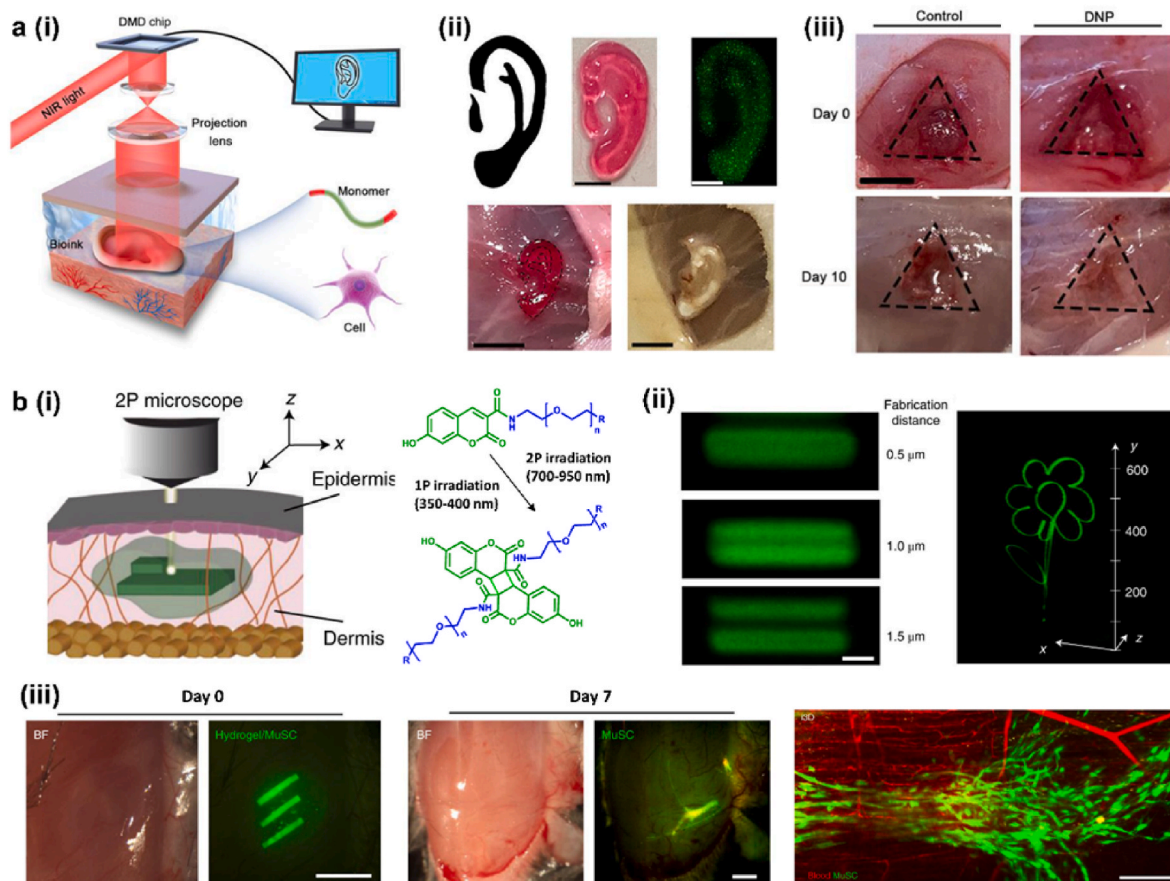
Fig. 3. a, Non-invasive *in vivo* bioprinting induced by NIR under digital micromirror device. (i) schematic diagram. (ii) NIR-induced *in vivo* bioprinting constructs high-fidelity, biocompatible ear-shaped gel structures (Scale bars: 2 mm (up), 5 mm (down)). (iii) *in vivo* bioprinting builds hydrogel that can repair volumetric muscle loss (Scale bar: 5 mm), adapted from Ref. [61], CC BY 4.0. **b,** Two-photon NIR induction enables intravital bioprinting. (i) schematic diagram and structural formula of the novel bioink. (ii) two-photon induction enables micron-level precision (Scale bar: 3 μm). (iii) *in vivo* bioprinting allows the construction of highly directional hydrogel structures inside the body to promote isotropic muscle growth (Scale bars: 1 mm (left and middle), 200 μm (right)), adapted, with permission from Ref. [62].

exhibit good cell viability with high speed and high resolution (Fig. 4a) [64,65]. Atala's team has conducted intensive research in droplet-based *in situ* bioprinting for skin wound repair. Among them, Skardal et al. carried out inkjet *in situ* bioprinting back in 2012 to print fibrinogen/collagen gels suspended with amniotic fluid-derived stem cells (AFS) and mesenchymal stem cells (MSC) onto the full-thickness skin wounds directly in mice [66]. Moreover, a trend toward faster healing was observed after three weeks compared to control groups. Further, the roles of paracrine cytokines of stem cells during bioprinted skin regeneration were revealed by cell tracking [67]. Based on the above studies, Albanna and colleagues have integrated a 3D laser scanner with droplet-based *in situ* bioprinting to develop a "mobile skin bioprinting system" that provides accurate topologies of skin defects for subsequent bioprinting treatment (Fig. 4b) [22]. The experiments on porcine models that printed autologous cells along with the fibrinogen-collagen hydrogel in the bilayer pattern revealed a 3-week acceleration in wound closure and re-epithelialization and 50% wound reduction in wound contraction.

Kerique et al. implemented laser-assisted *in situ* bioprinting for the deposition of nanohydroxyapatite/collagen-contained mesenchymal stromal cells inside a murine calvaria defect. The treatment success rate reached 29/30 after three months of observation, and little laser-induced neuroinflammation was detected (Fig. 4c) [68]. It is worth noting that the droplet-based bioprinting process requires relatively low-viscosity bioinks, which results in poor fidelity, integrity, and mechanical properties of the fabricated scaffold. Furthermore, the devices

associated with the bioprinting method are complex and challenging to miniaturize or integrate with internal surgical tools to treat deep and irregular-shaped defects [69]. Thus, it might be possible to improve its flexibility when used in conjunction with other bioprinting strategies, such as the extrusion/inkjet *in situ* bioprinting approach proposed by Moncal et al. (Fig. 4d) [70].

1.5. Bioink requirements for in vivo printing

During *in vivo* bioprinting, where the 3D structures are built and function in the physiological environment of the human body, it places additional requirements on bioinks beyond those needed for conventional *in vitro* bioprinting, as listed below.

(i) Rapid crosslinking and stable gelation in the intracorporal environment, including body temperature (37 °C), humid and dynamic tissue interfaces, and potential acidic microenvironment.

(ii) Possess flexible mechanical properties to resemble the native tissues to be repaired.

(iii) Possess adequate biocompatibility and controlled biodegradability, able to support cell proliferation, migration, and infiltration while serving as tissue scaffolds and degrade in parallel with tissue maturation.

(iv) Possess robust tissue adhesion for stable and long-term attachment to the moist and possible bleeding tissue surfaces in the defect microenvironment.
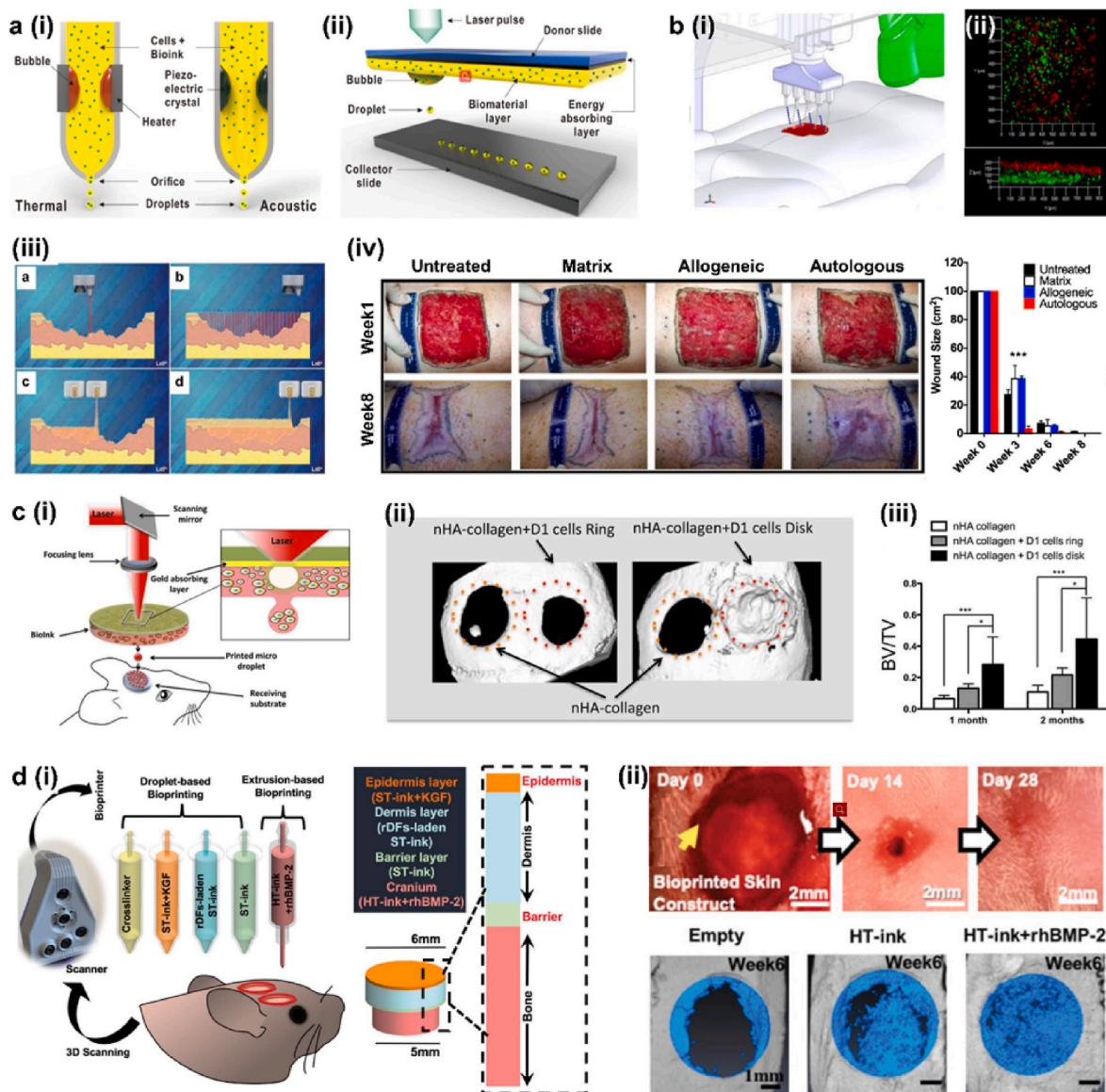
Fig. 4. a, Printing modalities capable of generating micro-droplets. (i) ink-jet bioprinting. (ii) laser-assisted bioprinting, adapted, with permission from Ref. [71]. **b,** The mobile skin bioprinting system based on ink-jet bioprinting for skin wounds repair. (i) schematic diagram. (ii) printed bilayer bionic structure containing the dermal (green) and epidermal (red) layers. (iii) laser scanning assists in the high-precision on-site management of extensive wounds. (iv) comparison of the effectiveness of different treatment methods for skin wounds (Untreated: control groups; Matrix: treated with fibrin and collagen solution alone; Allogeneic: treated with allogeneic cell-laden fibrin and collagen solution; Autologous: treated with autologous cell-laden fibrin and collagen solution), adapted from Ref. [22], CC BY 4.0. **c,** Laser-assisted *in situ* bioprinting to repair cranial injuries in mice. (i) schematic diagram. (ii) CT imaging results and (iii) statistics of the cranium after *in situ* bioprinting treatment, adapted from Ref. [68], CC BY 4.0. **d,** The composite bioprinting process of droplet-based and extrusion-based bioprinting for treating soft/hard tissue injuries in mice. (i) Schematic representation of the composite bioprinting process and the printed structure. (ii) representative photographs of skin and cranium tissue regeneration over six weeks post-surgery demonstrate primary recovery of composite tissue (Scale bars: 2 mm (up), 1 mm (down)), adapted, with permission from Ref. [70].

(v) One-step crosslinking and avoiding the post-treatment during gelation, minimizing the adverse effects on the physiological function of normal tissues.

Various bioinks used for *in vivo* bioprinting are summarized and evaluated in Table 1 according to the bioprinting modalities, bioink's biocompatibility, printability, bio-degradability, biomimetic mechanical properties, and wet tissue adhesion.

As described in the extrusion-based bioprinting section, the extrusion process has received the most academic attention due to its operational simplicity and broad applicability. In extrusion-based processes, a bioink initially present in bulk resting state, undergoes a transition to a high shear condition while passing through the nozzle, takes a new shape, and finally reaches a new resting state. The critical property for these transitions is printability, which refers to the "suitable" extrudability, filament formation, and shape fidelity. From a rheological perspective, ideal printability involves significant shear thinning, suitable yield stress, and reversible gel-sol transition behaviors [72,73]. This additional requirement for bioink ensures stable and high-fidelity of printed structures, which fulfills the high precision required for *in vivo* tissue repair.

Once the gel precursors have been extruded from the nozzle, additional crosslinking procedures are commonly needed to maintain their structures in intracorporal micro-environments. Photo-crosslinkable bioinks are the most widely used type of biomaterials for *in vivo* bioprinting due to their excellent properties and the ability to achieve

Table 1

Bioprinting modalities, bioinks and devices implemented for *in vivo* bioprinting.

No.	Printing modalities	Printing devices	Bioinks		Biomaterial's properties					Biological application	Ref
			Biomaterials	Cells and additional cytokines	Biocompatibility	Printability	Mechanical properties	Tissue adhesion properties	Biodegradable properties		
1	Extrusion-based Bioprinting (Photo-crosslinking)	Handheld device	GelMA + PEO	NIH/3T3 fibroblasts	Viability of 90%–95% in 7-day culture, with micropores for gas and nutrients transport	Acceptable	Not reported	Not reported	Degradable	None	[107]
2		Handheld device	GelMA + HAMA	IPFP stem cells	Viability of 95%–97% in 7-day culture	Acceptable, controllable	Storage modulus in 20 kPa after curing	Not reported	Degradable	None	[38]
3		Handheld device	GelMA + gelatin + HA	Osteosarcoma cell line Saos-2	Viability of 89% ± 10% in core and 84% ± 11% in shell	Acceptable, controllable	Storage modulus in 33 kPa–37kPa after curing	Not reported	Degradable	None	[39]
4		Handheld device	GelMA +	IPFP stem cells	Viability of 90% in 10-day culture, supports cell proliferation	Acceptable, controllable	Young's modulus in 195 ± 66.1 kPa	Not reported	Degradable	None	[25]
5			HAMA			Acceptable, controllable			Degradable	Repair for chondral defects in sheep	[40]
6		Handheld device	GelMA	C2C12 cells	Viability of >80% in 7-day culture, supports cell stretch, proliferation, and functional expression		Young's modulus in 30.6 kPa–42.4 kPa	Adhesive strength in 53–74 kPa with skeletal muscles	Degradable	Repair for VML injury in murine	[42]
7		Handheld device	GelMA	VEGF	Supports cell proliferation, migration, supports angiogenesis	Acceptable, controllable	Young's modulus in 1.2 kPa–10.6 kPa	Adhesive strength in 3.7–10.3 kPa with pig skin	Degradable	Repair for full-thickness skin wounds in porcine	[41]
8		Handheld device	GelMA + laponite	VEGF	Supports cell proliferation, migration, and functional expression	Acceptable	Young's modulus in 1.9 kPa–2.3 kPa	Adhesive strength in 2.3–3.1 kPa, and shear strength in 2.1–3.2 kPa with skeletal muscles	Laponite: Non-degradable [108]	Repair for VML injury in murine	[43]
9		Handheld device	GelMA + PVA		Supports cell proliferation, migration	Acceptable	Young's modulus in 30 kPa–130 kPa	Adhesive strength in 6–14 kPa with pig skin	Degradable	Repair for VML injury and subcutaneous implantation in murine	[44]
10		3-axis motion platform	GelMA/HAMA/PEGDA/NorHA	3T3 fibroblasts	Supports cell stretch with 88%–95% viability in 7-day culture	Favorable, construct tunable hydrogel filaments,	Not reported	Not reported	Degradable	None	[36]
11		3-axis motion platform	GelMA + Laponite + Methylcellulose	NIH/3T3 fibroblasts	Viability of 71%–77% in 21-day culture	Appreciable yield stress, shear-thinning response, high shape fidelity	Young's modulus in 104.7 kPa–139.2 kPa	Adhesive strength in 0.54–1.67 kPa with special interlocks	Degradable	None	[85]
12		3-axis motion platform	HAMA + PEGDA + Alginate		Not reported	Acceptable	Not reported	Not reported	Degradable		[109]

(*continued on next page*)

Table 1 (*continued*)

No.	Printing modalities	Printing devices	Bioinks		Biomaterial's properties				Biodegradable	Biological application	Ref
			Biomaterials	Cells and additional cytokines	Biocompatibility	Printability	Mechanical properties	Tissue adhesion properties	properties		
13		3-axis motion platform	GelMA + Cell-laden microgels	BMSCs	Support osteogenic differentiation with cell viability above 90%	Rapid photopolymerization	Compressive modulus in 3.73–204.0 kPa	Adhesive strength in 4–6 kPa with pig ribs	Degradable	Printing demonstration in *ex vivo* bone tissues Repair for osteochondral defects in murine	[92]
14		4DoF Robot Manipulators	GelMA + PEGDA + Alginate	MC3T3-E1 cells	Supports cell proliferation and up-regulated expression of osteogenic genes in 21-day culture	Rapid photopolymerization	Young's modulus in 78.1 kPa, compression limit in 33.89%; stress limit in 60.46 kPa	Not reported	Degradable	Repair for large segmental bone defects in swine	[110]
15		6DoF Robot Manipulators	HAMA	4-Armed PEG-ACLT	Supports cartilage defects repair, no immunogenic rejection reported	stable and accurate in high fidelity	Not reported	Not reported	Degradable	Repair for osteochondral defects in rabbits	[111]
16		7DoF Robot Manipulators	GelMA + PEGDA		Cell viability above 90% and low immunogenicity	Rapid photopolymerization in 1.5s	Compressive modulus in 35.2–254.7 kPa	Adhesive strength in 37.0 kPa with human tissues	Degradable	Repair for PROMs in rabbits	[112]
17	Extrusion-based Bioprinting (ionic crosslinking)	3-axis motion platform	Alginate + nanocellulose	Human chondrocytes	Viability decreases from 98% to 72% in 14-day culture, supports collagen type IIB expression	Acceptable	Not reported	Not reported	Degradable	Printing demonstration in *ex vivo* tibial tissues with osteoarthritis.	[113]
18		3-axis motion platform	Gelatin + Alginate	Fibroblasts	Potential cytotoxicity of calcium ion	Acceptable	Not reported	Not reported	Degradable	Not reported	[114]
19		3-axis motion platform	Poly-acrylamide	LiCl	Not reported	Acceptable	Tensile modulus in 8.7 kPa	Not reported	Microbial degradation only [115]	Printing demonstration on respiratory porcine lung	[116]
20		3-axis motion platform	Alginate + Pluronic F127	CaCl2	Potential cytotoxicity of calcium ion	Ordinary	Not reported	Not reported	Degradable	Not reported	[57]
21		3-axis motion platform	Alginate	CaCO3	Potential cytotoxicity of calcium ion	Acceptable	Young's modulus in 7.0 kPa–17.5 kPa	Not reported	Degradable	Not reported	[58]
22		3-axis motion platform	Alginate	CaSO4	Potential cytotoxicity of calcium ion	Acceptable	Not reported	Not reported	Degradable	Printing demonstration in *ex vivo* bone tissues	[117]
		MIS with RCM mechanism	Alginate + PEGDA	CaCl2	Not reported	Acceptable	Not reported	Not reported	Degradable	Printing demonstration on *ex vivo* ovine humerus	[118]
23		MIS with mini-bioprinting platform	Gelatin + Alginate	GES-1 and HGSMCs	Viability of 90% in 10-day culture	Acceptable	Not reported	Not reported	Degradable	Printing demonstration in special-fabricated stomach model	[119]
24	Extrusion-based Bioprinting (enzymatic crosslinking)	Handheld microfluidics device	Alginate + collagen, fibrinogen + HA + collagen	Human dermal fibroblasts and epidermal keratinocytes, thrombin	Viability of 90% in 10-day culture, supports cell proliferation, and functional expression	Ordinary	Vulnerable	Not reported	Degradable	Repair for full-thickness burn injury in porcine	[51]
25			Fibrinogen + HA	MSCs		Ordinary	Vulnerable	Not reported	Degradable		[52]

Table 1 (*continued*)

No.	Printing modalities	Printing devices	Bioinks		Biomaterial's properties					Biological application	Ref
			Biomaterials	Cells and additional cytokines	Biocompatibility	Printability	Mechanical properties	Tissue adhesion properties	Biodegradable properties		
		Handheld microfluidics device			Viability of 95% in 7-day culture, supports cell proliferation, and functional expression					Repair for full-thickness skin injury in porcine	
26		4DoF Robot Manipulators	self-assembling peptides: IVZK and IVFK	HDFn and hBMSCs	Supports faster cell proliferation and minimal gene expression differences	Acceptable, relies on microfluidic units	Storage modulus in 6 kPa–100 kPa at different peptide concentration.	Not reported	Enzymatic degradation	Not reported	[120]
27	Extrusion-based Bioprinting (thermo crosslinking)	3-axis motion platform	Collagen + Chitosan + n-HA	rBMSCs, β-GP + BMP2 + PDGF	Supports cell migration and proliferation, promotes differentiation towards osteoblasts and calcium ion deposition.	Favorable	Not reported	Not reported	Chitosan: Depends on the degree of deacetylation [121] n-HA: Non-degradable	Repair for calvarial defects in murine	[55]
28		6DoF closed-loop Robot	Matrigel	Epi-SCs, SKPs	Viability of 90% in 7-day culture, supports cell proliferation, and functional expression	Ordinary	Not reported	Not reported	Degradable	Repair for full-thickness skin wounds in murine	[122]
29	Extrusion-based Bioprinting	3-axis motion platform	PCL + ZnO +HA		Antimicrobial, bio-inert, supports cell proliferation and differentiation	Ordinary	Young's modulus in 180 kPa	Adhesive strength in 216–297 kPa	Degradable	Printing demonstration in *ex vivo* porcine bone and murine calvarial defect. And subcutaneous implantation in murine	[56]
30		MIS with ferromagnetic soft catheter robot	HA + Pluronic F127	PEDOT: PSS + polycarbophil	Not reported	Acceptable	Not reported	Not reported	Degradable	Printing demonstration on a rat liver	[123]
31		3DoF closed-loop Delta robot	Sliver + PEO		Not reported	Acceptable	Not reported	favorable after 1000 cycles of bending	Sliver: Non-degradable	Printing on a moving hand and a living murine	[124]
32	SLA-based bioprinting	Digital micromirror device	GelMA	Articular chondrocytes, and ASCs, UCNP@LAP	>80% cell viability in 7-day culture	Acceptable	Not reported	Not reported	Degradable	Repair for muscle defects in murine	[61]
33		Multi-photon microscope	HCC-PEG, HCC-gelatin	HUVECs, hESCs, fibroblasts	Viability of 90%–99% in 3-day culture, supports cell stretch, proliferation, and functional expression	Acceptable	Young's modulus in 1 kPa–20 kPa	Not reported	Degradable	Printing demonstration inside murine dermis, skeletal muscle, and brain	[62]
34	Droplet-based Bioprinting (ink-jet droplets)	Handheld device	Collagen + fibrinogen + agarose	hDPCs, thrombin	Supports cell functional expression	Ordinary	Not reported	Not reported	Degradable	Printing demonstration within bovine teeth	[125]
35		3-axis motion platform	Collagen+Fibrinogen	AFS cells, and MSCs, thrombin	Supports cell proliferation,	Ordinary, frequent clogging of the printhead	structural integrity Inferior mechanical	Not reported	Degradable	Repair for full-thickness skin wounds in murine	[66]

Table 1 (*continued*)

No.	Printing modalities	Printing devices	Bioinks		Biomaterial's properties					Biological application	Ref
			Biomaterials	Cells and additional cytokines	Biocompatibility	Printability	Mechanical properties	Tissue adhesion properties	Biodegradable properties		
					differentiation and functional expression		properties due to incomplete structural integrity				
36		3-axis motion platform	Thiolated HA + thiolate gelatin + PEGDA	AFS cells	Supports cell proliferation, differentiation and functional expression	Ordinary, frequent clogging of the printhead	Not reported	Not reported	Degradable	Repair for full-thickness skin wounds in murine	[67]
37		3-axis motion platform	Collagen + Fibrinogen	Autologous dermal fibroblasts and epidermal keratinocytes, thrombin	Supports cell proliferation, and functional expression	Ordinary, frequent clogging of the printhead	structural integrity Inferior mechanical properties due to incomplete structural integrity	Not reported	Degradable	Repair for full-thickness skin wounds in murine, and swine	[22]
38		3-axis motion platform	Fibrinogen	Endogenous stems cells, thrombin	Not reported	Ordinary, frequent clogging of printhead	Not reported	Not reported	Degradable	Repair for calvaria defects in murine	[126]
39		4DoF Robot Manipulators	PEGDA		Not reported	Acceptable	Young's modulus in 0.77 ± 0.006 MPa	Not reported	Degradable	Printing demonstration on a mouse model	[127]
40	Droplet-based Bioprinting (Laser-assisted droplets)	High-throughout laser printer	n-HA		Not reported	Acceptable	Not reported	Not reported	Non-degradable	Repair for calvaria defects in murine	[69]
41		High-throughout laser printer	collagen, n-HA	MSCs	Not reported	Acceptable	Not reported	Not reported	n-HA: Non-degradable	Repair for calvaria defects in murine	[68]
42		High-throughout laser printer	collagen	HUVECs, VEGF	Supports cell proliferation, and functional expression	Acceptable	Not reported	Not reported	Degradable	Repair and vascularization for calvaria defects in murine	[23]
43	Extrusion-based/ Droplet-based Composite Bioprinting	3-axis motion platform	Collagen + Chitosan + nHA, collagen + fibrinogen	rBMSCs, β-GP + BMP2+PDGF, KGF	Supports cell migration and proliferation, promotes tissue regeneration	Acceptable	Young's modulus in 8.2 ± 1.4 kPa for hard tissues, and 1.7–2.39 kPa for soft tissues	Not reported	n-HA: Non-degradable	Repair for composite calvarial bone and skin defects in murine	[70]

bioprinting for deep tissue repair through the modulation and conduction of light [74]. There are also studies into the material modification to confer the photo-crosslinking capacity to hydrogels by grafting photo-initiating groups for printability improvement. For instance, hyaluronic acid (HA), another widely used bioink for bioprinting, provides an ECM-like microenvironment [75], and its photo-crosslinkable derivatives, HAMA [76–78], improves the vulnerable soft texture and slow crosslinking of the bioink. Similar cases include methacryloyl-alginate [79,80] (AlgMA), chitosan methacrylate [81] (CSMA), etc. Meanwhile, these photo-responsive bioinks can also be applied well in the stereolithography-based bioprinting.

In the droplet-based bioprinting process, manipulating cells with picolitre-scale droplets provides an advantage in constructing subtle tissue structures. Collagen and fibrinogen are the common bioink materials used for droplet-based bioprinting due to their recapitulation of extracellular matrix upon crosslinking. Furthermore, these biomaterials can incorporate various cells to recapitulate complex multicellular tissues, including skins [22,66]. Notably, nozzle clogging has been a challenge that has plagued the development of the inkjet bioprinting process, a mainstream droplet generation approach, which has limited the viscosity of bioink for inkjet bioprinting to relatively low levels, generally in the range of 3–30 mPa s^{64}. Laser-assisted bioprinting, another approach for creating microdroplets, is broadly inclusive regarding the viscosity of bioinks (1–8000 mPa s) [65]. Nevertheless, the preparation of bioink into laser-absorbed targets remains challenging and makes the options for bioinks cumbersome.

Focusing again on GelMA, the commonly used bioink during *in vivo* bioprinting, while presenting positive in all other evaluation dimensions, the tissue adhesion mainly derived from hydrogen bonding between free hydroxyl groups in the hydrogel structures and tissues barely satisfactory [82,83]. Favorable tissue adhesion is essential for improving implantation and eventual tissue integration of engineering scaffolds to prevent post-surgical dislocation and functional failures. For the wet tissue surfaces and bleeding interfaces common in intracorporal defects, it is not sufficient to rely solely on intermolecular forces between the hydrogels and tissues to maintain adhesion. The intuitive solution is to reinforce the connection through suturing, while it raises the risk of structural disruption due to stress concentrations at the sutures [84]. Interestingly, it has been reported that *in situ* printing of unique structures such as hydrogel rivets can establish a solid adhesion to different tissues through physical interlocking [85]. Tissue adhesion has also been reinforced by constructing microgel bioink, a binary material system popular in controlled drug release [86], disease modeling [87], etc. Benefiting from unique rheological properties similar to Bingham fluids, microgel bioink displays as elastomer below certain stress and exhibits Newtonian fluidity once the stress is further increased [88,89]. While improving printability, micro-components presence expands the contact area between the biomaterials and living tissues, allowing reactive groups in the hydrogels, such as N-hydroxysuccinimide [90] or dopamine groups [91], to establish a complete bonding in the tissue interface. Xie et al. developed a bioconcrete bioink for *in vivo* bioprinting, in which the cement component easily infiltrates the wound surface and forms high internal friction and hydrogen bonds on the defect-hydrogel interface, presenting adequate adhesion even in bleeding surfaces [92].

More research is now focusing on enhancing the tissue adhesion of bioinks via different physiochemical mechanisms [83]. Such as in injectable hydrogels, most rely on the mussel-inspired strategy. Therein catholic polymers are naturally generated [93] and subsequently oxidized into the strongly adhesive dopamine [94], forming various covalent and non-covalent interactions penetrating the interfacial water and achieving stable wet tissue adhesion [95,96]. Moreover, a covalent bond can be achieved via the interaction of the amine groups in poly (acrylic acid) grafted with N-hydroxysuccinimide ester [97] (PAA-NHS ester) with the free carboxylic acid groups on various tissues [98–100], or by the methacrylate groups in photo-crosslinkable bioinks such as

GelMA with the amino groups on cardiac tissues [101]. These adhesion groups could be further strengthened through *in situ* polymerization since the chemical anchors in the hydrogel network interpenetrate with the substrate. However, it is noteworthy that the enhanced tissue adhesion due to materials modification might compromise other properties, such as the deteriorated printability due to altered rheological properties [102], prolonged crosslinking period [103], and unidentified immunogenicity and cytotoxicity [104–106]. Thus a trade-off between properties is necessary, aiming at the specific requirements for tissue injury repair.

1.6. Devices and systems for in vivo bioprinting

The printing devices and systems complement the bioprinting modalities and can be regarded as the mediums through which the bioprinting functions inside the body. Bioprinting devices used for fabricating scaffolds directly inside the patient's body can be divided into two major categories: handheld bioprinting devices and frame-based multi-axis platforms.

1.7. Handheld bioprinting devices

The handheld bioprinting devices involve a highly portable device with a bioprinting unit that allows the deposition of bioinks with a programmed rate in a direct-write approach, while the movement and positioning of bioprinting are provided manually by the surgeon.

Several handheld *in situ* bioprinting devices have been reported and implemented for the treatment of tissue injuries, including bone [128, 129], cartilage [25,40], dental pulp [125], skin [41,130], and muscle [42,43,131]. Among them, the ongoing and long-term studies include the "Biopen" proposed by Bella's group [25,38–40], which spent five years progressing from prototype development and exploration of printing parameters to coaxialization improvements of the printhead and evaluation of biological metrics (Fig. 5a), culminating in a promising application in cartilage injure repair in sheep [40], demonstrating the application potential for tissue defects repair of *in vivo* bioprinting. Coincidentally, researchers from the University of Toronto have also implemented three iterations of the microfluidics-based handheld bioprinter to meet the needs of clinical use [51,52]. They introduced a guiding wheel to match the speed of manual movement and the extrusion speed, which overcame the inconsistency in manual bioprinting and optimized biomaterial drift due to gravity on inclined surfaces (Fig. 5b) [52]. In porcine pre-clinical models of full-thickness burn, the bioprinter delivered cell-containing fibrin sheets directly on the wound bed, improving re-epithelialization and neovascularization [52].

Most other handheld bioprinting devices have relied on extrusion-based *in vivo* bioprinting methods, probably due to the challenges associated with the miniaturization of other bioprinting approaches, such as SLA and DBB.

The subject of the handheld bioprinting devices is the surgeon that able to adjust the printing locations according to the actual situations of the defects, such as unintended variations in the position and shape of the wounds due to breathing and changes in wound geometries induced by preoperative debridement, which enables a targeted treatment for tissue injuries (Fig. 5c). The smaller profile and reduced infrastructure needed for handheld bioprinters facilitate their sterilization and increase their portability. Nevertheless, the clinical application of handheld devices is still essentially a surgical operation and acts as an extension of the clinician's hand. Thus it faces challenges in terms of resolution and precision, and the therapeutic outcome varies depending on the practitioner's skills. Restricted operational space for internal tissue repair is another challenge, and it is ordinarily necessary to create additional incisions to provide sufficient areas for the surgical procedure. As such, current handheld bioprinting devices fail to address the need for large-scale composite tissue defects.
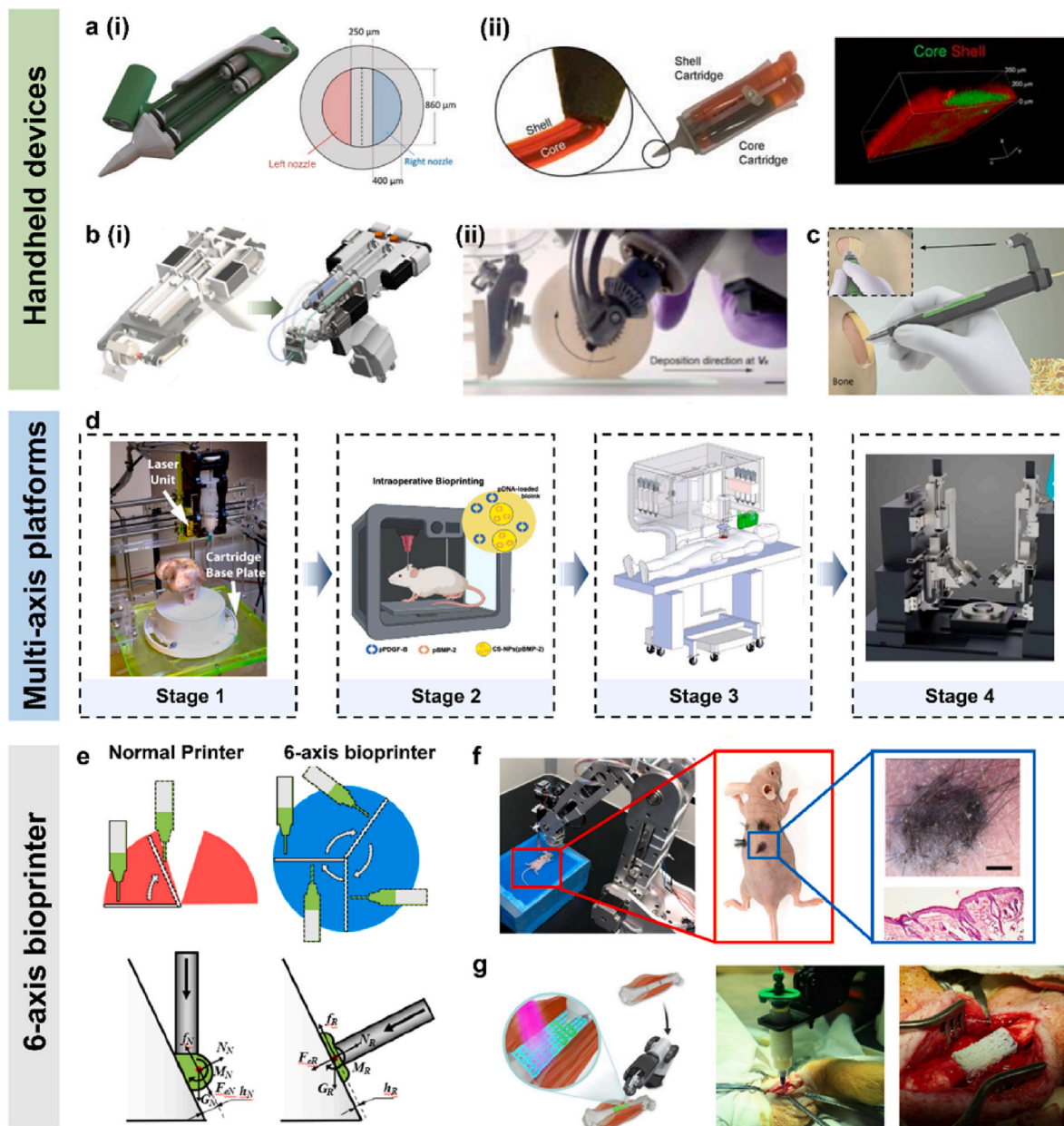
Fig. 5. a, Handheld bioprinting device "Biopen" developed by Bella's group. (i) primary prototype with two ink cartilages and the parallel nozzle, adapted, with permission from Ref. [38]. (ii) modified device with a coaxial nozzle enables the printing of coaxial hydrogel filaments with high-fidelity, adapted from Ref. [25], CC BY 4.0. **b,** The microfluidics-based handheld bioprinter developed by the University of Toronto. (i) iterative evolution of the device. (ii) the designed guide wheel enables the match of the printing speed and the extrusion speed, adapted, with permission from Ref. [52]. **c,** The integrated camera in the handheld device captures the image of the print view, adapted, with permission from Ref. [56]. **d,** Representative images of multi-axis bioprinting platform in different stages of development. Stage 1, the proof of concept for *in vivo* bioprinting on *ex vivo* tissues, adapted, with permission from Ref. [117]. Stage 2, *in vivo* bioprinting exploration on living small animals such as mice, adapted, with permission from Ref. [55]. Stage 3, attaching portable castors to the frame-based structure that allows it to address large areas of injured tissues, adapted from Ref. [22], CC BY 4.0. Stage 4, introducing degrees of freedom at the printhead in the frame-based structure to accommodate complex surfaces. **e,** Comparison of the feasible printing angles o the printhead and morphological analysis of the printed structures between the conventional bioprinter and the 6-axis bioprinting robot, adapted from Ref. [122], CC BY 4.0. **f,** The 6-axis adaptive bioprinting robot performs *in situ* bioprinting to treat skin injuries in mice, and the regenerated skin contains accessory organs including hair follicles (Scale bar: 2 mm), adapted from Ref. [122], CC BY 4.0. **g,** 6-axis *in situ* bioprinting guided by structural light scanning reconstruction to repair large segments of bone defects, adapted from Ref. [110], CC BY-NC-ND.

1.8. Frame-based multi-axis bioprinting platform

The frame-based multi-axis platform is the most commonly used device in 3D bioprinting research, where the bioinks are automatically distributed and deposited following the predefined structure to fabricate tissue scaffolds (Fig. 5d). Combined with different printing units, such as extrusion mechanisms, print cartridges, etc., these devices can be adapted to different *in vivo* bioprinting modalities. Over the past decade,

the application of frame-based platforms for *in vivo* bioprinting has significantly evolved owing to its robust structure and simplicity. In 2010, Cohen et al. demonstrated *in vivo* bioprinting by performing *in situ* bioprinting for both chondral and osteochondral defects created on the isolated calf femur, and favorable printing precision was acquired in conjunction with computerized tomography (CT) scanning [117]. In the next stage, scholars investigated *in situ* bioprinting on small animals, such as full-thickness skin wounds and cranial defects in mice [55,66,67,

126], which also presented promising results. Additionally, they attached several passive wheels to the frame-based device, further enhancing the portability and extending the device's range of motion to enable *in vivo* bioprinting for large wounds [22].

As an automated device, the frame-based motion platform offers higher printing accuracy and fewer human errors than manual operation, while it is still limited when applied in deep tissue repair. The effective workspace of the frame-based devices is always inside their structures, resulting in a disturbing space utilization [122,132]. Most commercially available stationary bioprinters are small and incapable of hosting a human body or body part, and it is challenging to be miniaturized for integration with minimally invasive internal surgery tools. Consequently, the bioprinting studies involving animal experiments with these devices are generally confined to superficial tissue injury repairs, such as skin [22,66,67] and calvaria [23,55,70,109]. In addition, the existing frame-based platforms mainly possess three degrees of freedom (DoF), thus their printheads are fixed vertically downwards in most cases [122]. This configuration assumes a horizontal plane in bioprinting, which is incompatible with the complex surface morphology of tissue defects in practical [133]. The printing nozzle's fixed orientation is not sufficient for the *in situ* tissue repair of complicated surfaces. Hence, it was hoped that additional DoF could be added to the printhead to address the challenges for curved, angled surfaces [110,120,127,134], yet again this would not eliminate the inherent deficiencies of the frame-based structure.

A strategy to address the requirements for workspace and DoF is the implementation of robot-assisted *in vivo* bioprinting [111,122,135]. Industrial manipulators with six DoFs have been widely used in the manufacturing industry and are emerging in 3D printing for metals [136] and architectures [137]. Due to their increased DoFs and serial mechanism property, the manipulators possess a higher workspace/occupied-space ratio and offer access to the defective corners with high precision in specific orientations (Fig. 5e) [122]. In contrast to other printing applications, such as metals, where the printed object is homogeneous and nonliving with high rigidity, *in vivo* bioprinting works on dynamic and vulnerable human tissues. It demands precise control of contact force with tissues during contact bioprinting, such as extrusion-based modality, which would otherwise lead to secondary injury to the defects. Zhao et al. integrated binocular vision with a six-axis manipulator to propose an adaptive bioprinting robot that offers precise recognition [122], rapid kinematic response, and adaptability to diverse surfaces. Combined with stem cell-laden bioinks, they performed *in vivo* bioprinting on the backs of live, wounded mice and realized the regeneration of functional skin tissue containing appendages such as hair follicles (Fig. 5f). This shows the generality of this adaptive bioprinting system for tissue injuries repair in clinical settings. Similarly, the robotic printed repair of bone defects has also been explored by scholars (Fig. 5g). Despite possessing six DoFs, the robot-assisted bioprinting is inadequate in compliant control [138], i.e., there only exists one configuration relating to a targeted position, which might lead to unintended collisions with the surrounding. This technology is still under development and requires advances in manipulator control to facilitate the progress of *in vivo* bioprinting.

1.9. Device explorations combining with minimally invasive surgery

The demands for *in vivo* bioprinting devices involve minimally invasive, large workspace, adaptability to deep tissues, and high precision, which makes us naturally associated with minimally invasive surgical tools. They are inserted into the patient to assess the intracorporal defects through a small incision, where surgical tools must pivot and translate around, to pattern a remote center of motion (RCM) (Fig. 6a) [139,140]. The RCM motions can be achieved in a passive approach that guarantees the mechanism's end-effector always passes through a spatially fixed point via linkage constraints. The passive RCM mechanisms have been extensively developed and modified since 1992

[141] when it was successfully applied in clinical minimally invasive surgery (MIS). Among them, the most representative da Vinci surgical system of Intuitive Surgical, Inc. implemented the RCM operations based on the parallelogram mechanism that presents more compact and flexible [142]. The restraint of the mechanism guarantees the invariance of the RCM point and further ensures safety during the operation procedure, which is essential in surgery. Inevitably, this also brings limitations, as the location of the RCM point is non-adjustable once the linkage length has been determined. The researchers introduced multiple driven joints in the mechanism to match the RCM points with the patient's incision, but this led to a cumbersome alignment procedure before clinical surgery [139,143]. Lipskas et al. developed a minimally invasive bioprinting device based on a spherical RCM mechanism [118] that enabled contact scanning, milling, and *in situ* bioprinting on a cartilage model through different substitutable end-effectors, which demonstrated the potential of the RCM mechanism for *in vivo* bioprinting (Fig. 6b).

In contrast to the passive RCM approach, RCM movements can also be generated by a 7-DoF serial robot system through the proper controller design, thus known as the active RCM approach [144–146]. The extra DoF confers redundancy and better dexterity to the conventional 6-axis bioprinting robot above and further leads to diverse configurations in the limited workspace, making the 7-DoF manipulator a promising option for minimally invasive internal bioprinting strategies. Nevertheless, current research mainly focuses on theoretical studies such as controller design for RCM motions [147–150], while lacking obvious application footholds and correlational advances in bioprinting. An innovative study conducted by Zhao et al. recently proposed a novel strategy that combines the 7-DoF manipulator and subaqueous bioprinting to achieve initial therapeutic effects for premature rupture of membranes in animal studies, further presenting the potential of the 7-axis robot in intracorporal bioprinting [112]. However, it should be aware that the spatial immobility of the active RCM mechanism is virtual and never as robust as that of the passive RCM mechanisms, where the immobility point relates only to the design parameters of the mechanism's linkage [151]. In medical procedures, ensuring safety must be prioritized, which has led to current surgical robots based chiefly on passive RCM mechanisms [152]. In the further development of active RCM devices, challenges for risk reduction remain and need to be addressed through research into more reliable safety control strategies.

In the minimally invasive *in vivo* bioprinting studies described above, the printing nozzles are rigid and driven by the mechanism while moving. An innovative study reported recently differs from the mechanically driven approach that proposed a nozzle-deformation-based bioprinting strategy through a ferromagnetic soft nozzle [123]. The novel nozzle is designed to access the internal tissues through a small incision, which acts as a channel for bioink extrusion, and deforms under a programmable magnetic field to print the desired structures. This approach successfully demonstrated *in situ* bioprinting on *in vitro* models, isolated heart tissues, and a living rat liver (Fig. 6c).

Natural orifice transluminal endoscopic (NOTE) bioprinting is another desirable method for internal tissue repair that is free from the incision. However, the inverse kinematics of the endoscopic robot has been reported as a common challenge in the fields of flexible serial robots [153,154], thus it is difficult to achieve *in vivo* bioprinting with the endoscopic robot alone. Zhao et al. have designed a miniature bioprinting platform inspired by an origami structure, which only needs to be delivered to a specific location inside the body through an endoscope and to carry out subsequent precision bioprinting in the defects (Fig. 6d) [119]. Origami-inspired mechanisms combined with micro-electro-mechanical system (MEMS) processing can solve the control puzzles in the NOTE robot and offers a promising solution for creating miniaturized mechanisms. Based on these principles, mini-scale bug robots [155–157] and even mini-RCM surgical robot [158] have been developed, which could provide valuable insights for *in vivo* bioprinting devices.
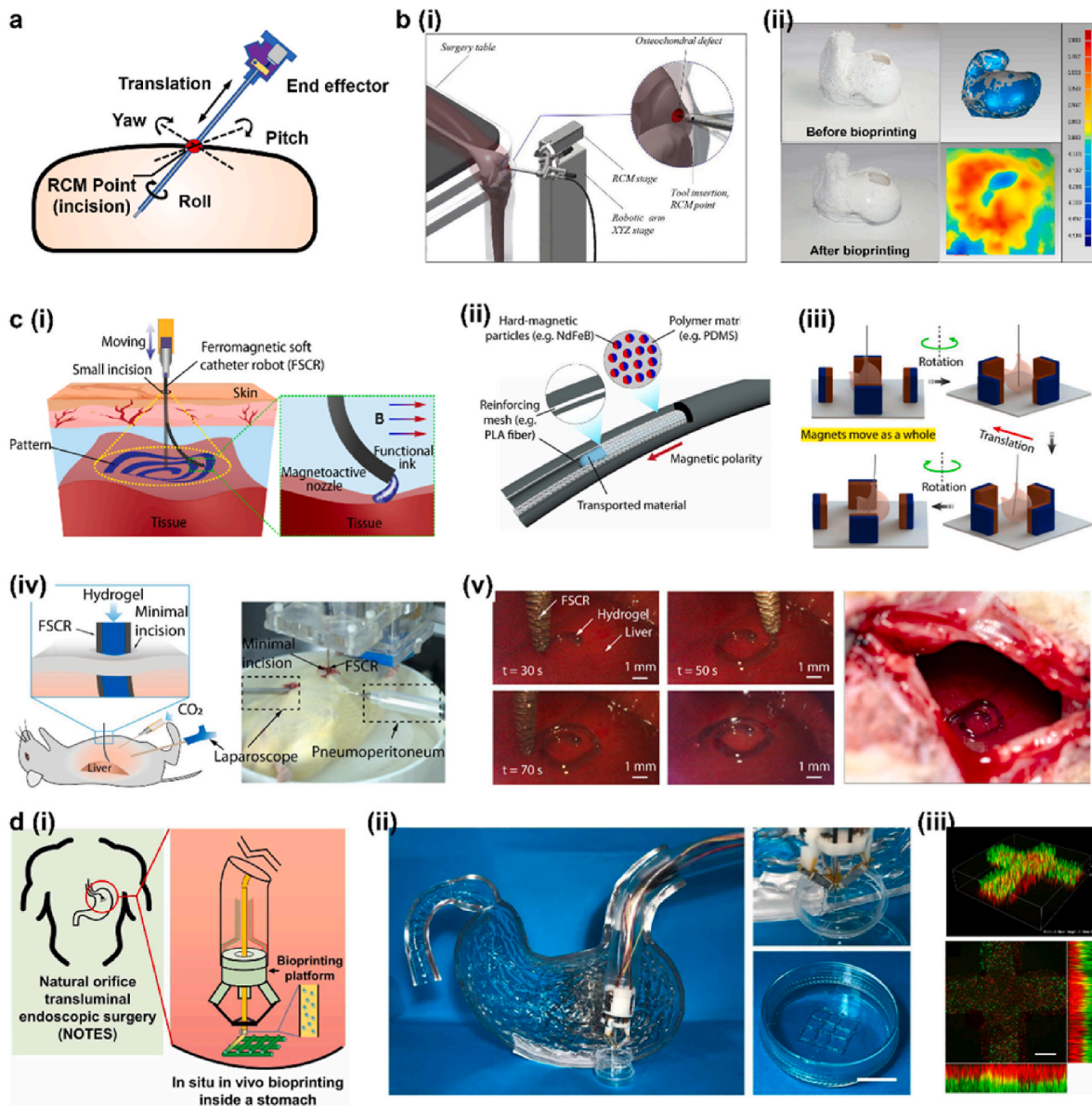
Fig. 6. a, Schematic diagram of the minimally invasive surgery. Due to the limitations of the RCM point, the surgical instrument has only 3 DoFs in rotation and 1 DoF in translation, adapted, with permission from Ref. [112]. **b,** Minimally invasive *in vivo* bioprinting device based on passive RCM mechanism for repairing cartilage injuries. (i) schematic diagram. (ii) comparison of the model after bioprinting and before damage presents a superior printing accuracy, adapted from Ref. [118], CC BY 4.0. **c,** The ferromagnetic soft catheter robots for minimally invasive bioprinting. (i) schematic diagram of magnetron *in vivo* bioprinting. (ii) schematic of the robot composed of a soft polymer matrix with dispersed hard-magnetic particles and PLA reinforcing mesh. (iii) the numerical control strategy of the robot, where operations are instructed by digital data. (iv) schematic illustration and images of the experimental setup for the *in vivo* experiment. (v) the process of minimally invasive bioprinting at different times (Scale bars: 1 mm), adapted from Ref. [123], CC BY 4.0. **d,** The *in situ in vivo* bioprinting strategy via the natural cavity to repair gastric damage. (i) schematic diagram. (ii) the bioprinting setups and the printed structures (Scale bar: 1 cm). (iii)Fluorescence micrographs of the printed structure, which contains a bilayer structure representing the epithelial (green) and muscular layers (red) of the stomach, respectively (Scale bar: 500 μm), adapted, with permission from Ref. [119]. In addition to the academic field, commercial bioprinters are flourishing in the industry. However, owing to the specific properties of *in vivo* bioprinting, most reported bioprinters are laboratory-developed versions with few commercial systems currently available [32]. Some examples include the integration of machine vision with the Fab@Home Model3 platform investigating path planning during *in vivo* bioprinting [114] and upgrading the Regenovo Bio-Architect bioprinter with in-situ photo-crosslinking printheads [109]. Similarly, in serial mechanisms, scholars further advanced the applicability of commercial multi-DoF manipulators in intracorporeal operations through combination with specially designed printing end-effectors, such as Dobot [111] (Shenzhen, China), Universal Robot [110] (Odense, Denmark) and BioAssemblyBots (Louisville, USA). Although few commercial bioprinters can yet be directly applied to *in vivo* bioprinting research, their rapid development has shown us the glimpses to come. Recent commercial bioprinters have become available with optional modules, including coaxial flow-focusing technology (Aspect Biosystems RX1), *in situ* crosslinking tool head (CELLINK), and pneumatic spraying (Aether 1), which allows for convenient migration to *in vivo* bioprinting studies. More comprehensive overviews of commercial bioprinters can be found elsewhere [159–161]. Commercial bioprinters with various properties are available for the needs of different scholars and will together contribute to the advancement of *in vivo* bioprinting.

2. Integration with clinical procedures for *in vivo* bioprinting

Through the studies of *in vivo* bioprinting modalities, bioinks, and devices, a blueprint of this emerging technology applied to tissue repair has been laid out, and research in the integration with clinical procedures is indispensable to turn the blueprint into a reality that benefits tissue injuriy repair. The open intraoperative setting where the bioprinting is performed clinically puts demands at different stages, such as rapid planning before bioprinting, dynamic response during bioprinting, and stimulation regulation after bioprinting, to pursue the efficient, accurate, and functional recovery therapeutic implementation of *in vivo* bioprinting.

2.1. Pre-bioprinting stage

The procedures prior to *in vivo* bioprinting include the 3D reconstruction of tissue defects, tissue segmentations, and planning of conformal printing path, etc., among which the perception and re-establishment of the injured tissues is the basis for the subsequent process. Table 2 summarizes some 3D perception methods that capture the target surface geometry. The structure to be printed is often obtained by Boolean subtraction [162,163] between the defect's surface geometry and a model of the original tissue, which is commonly unknown and can be addressed through symmetry or smooth interpolation. In the studies related to *in vivo* bioprinting, Cohen et al. applied the volumetric reconstruction technique, i.e., computed tomography [117] (CT), to obtain a model of calf femur while eliminating using sophisticated algorithms for 3D encapsulation in other surface-based methods (Fig. 7a). Laser scanners and structured-light scanners are the versatile methods for printing tissue scaffolds (Fig. 7b) [109,164] and even organ chips [165], such as the conformal microfluidic chip fabricated on a kidney surface to extract renal metabolic and pathological markers. Despite the high resolution and accuracy, these scanning methods might be ineffective in some surgical scenarios, such as specular reflection on wet tissue surfaces. Stereo vision scanners strike a balance between scanning speed and accuracy that most closely match the needs of *in vivo* bioprinting that reflects in real time the actual target geometric and kinematic states, thus can readily adapt to dynamic and non-planar surfaces with high precision. Given this availability of stereo visual systems [166], various algorithms for camera calibration [167], feature detection [168], and real-time tracking [169,170] can be transferred from the laboratory to the medical-imaging domain. Still, there are fewer investigations associated with bioprinting reported.

The random and complicated nature of wounds makes it common for the reconstructed models to contain multiple types of tissues, thus making it essential to proceed with a segmentation procedure based on tissue categorifies. A straightforward approach is to detect the signal gradient of different tissues, which has been integrated into Materialise's interactive medical image control system (MIMICS, Belgium), a widespread clinical software for CT, MRI, etc. However, it often relies on human assistance for judgement and decision-making, such as sketching contour lines. Deep learning has also been incorporated into tissue differentiation, such as convolutional neural networks (CNN), to pursue an accurate anatomical segmentation with minimal human intervention (Fig. 7c) [173]. Meanwhile, new multi-modal perception strategies are being developed parallel for tissues with similar visual features, such as colors and textures [174–176]. Raizman et al. performed fluorescence imaging for bacteria in skin trauma in addition to optical imaging to achieve targeted debridement that is challenging through binocular vision alone [177].

Once the 3D model with onefold tissue is obtained, it must be layered to create the printing path. Conventional 3D printing relies on a planar-based layering, while as Lian et al. identified [178], the plane layering wound not only results in interruptions in the printing path but also bring flaws and severe step effects (Fig. 7d), which affects the conformality of the fabricated structure and the attachment with tissue defects. In contrast, the conformal slicing method, where each layer's trajectory has a similar profile to the tissue defect, can address these difficulties and promise to maintain the isotropic growth of the regenerated and native tissues in composite tissue repair (Fig. 7e) [179]. The spatially conformal path generated based on planar path projections can also fulfill a similar purpose [122,180,181], while it is only appropriate for the printing of single-layered scaffolds (Fig. 7f). All the studies above together provide rapidity in preoperative preparation.

2.2. Bioprinting stage

In the intraoperative implementation of *in vivo* bioprinting, maintaining high precision and accuracy is significant for the treatment and postoperative recovery. Among them, precision implies the variation between several bioprinting attempts and represents the stability of the printing process, while accuracy refers to the level of agreement between the printed structures and the desired state, similar to printing conformality. Both can be accomplished by introducing a feedback system into the conventional open-loop 3D bioprinting.

In terms of improving printing precision, closed-loop control is required due to disturbances in the printing environment, and uncertainties in material properties and mechanical behaviors. By integrating various sensors into the printing platform, the states of bioinks and printing defects in fabricated structures were observed and fed to

Table 2
Common 3D perception methods associated with bioprinting.

| Method	Resolution	Accuracy	Speed	Pros	Cons	Refs
Computed tomography	Medium	Medium	Slow	Enables volumetric reconstruction	Radioactive, bulky equipment and slow perception scanning speed	[55,68–70,110, 111,113,117, 123]
Magnetic Resonance Imaging	Medium	Medium	Slow	Enables volumetric reconstruction and identification for wide range of soft tissues	Bulky equipment and extremely slow scanning speed	[23,113]
Trilinear coordinates measuring instrument	High	High	Slow	Contact-based measurement, adaptable to various surfaces	Point-based scanning, and prolonged scanning time as resolution increases	[118,171]
Laser scanning	High	High	Medium	Portable, suitable for a wide range of dimensions	Expensive equipment, Ineffective for transparent or reflective surfaces	[22,66]
Structured-light scanning	High	High	Medium	Portable, relatively cheap equipment	Ineffective for transparent or reflective surfaces; performance affected by ambient lighting	[109,113,116, 124]
Binocular visual system	Medium to High	Medium to High	Fast	High adaptability to object targets, low cost	Ineffective for transparent or reflective surfaces, high requirements for recognition algorithms	[114,116,122, 124]
Optical coherence tomography	High	High	Medium	Extremely high precision, and Independent of ambient lighting	Limited scanning area and only adaptive for objects with particular features	[172]
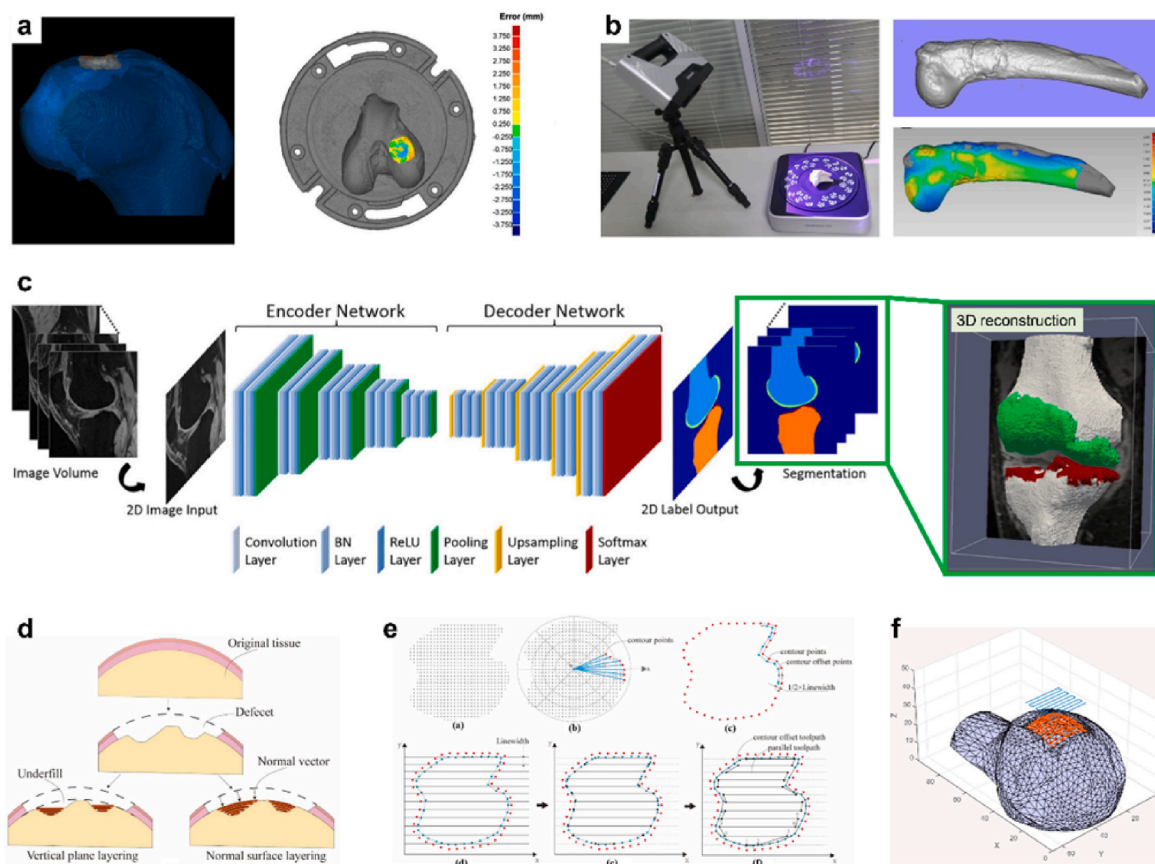
Fig. 7. a, Scanning and accuracy assessment of the femoral head before and after bioprinting treatment using CT, adapted, with permission from Ref. [117]. **b,** Scanning and accuracy assessment of the tibial model before and after bioprinting treatment using laser 3D scanning, adapted from Ref. [109], CC BY 4.0. **c,** A new fully automated musculoskeletal tissue segmentation method using deep convolutional neural network (CNN) and 3D simplex deformable modeling to improve the accuracy and efficiency of cartilage and bone segmentation within the knee joint, adapted, with permission from Ref. [173]. **d,** Schematic comparison of the performance of the vertical plane layering and the normal surface layering for filling the tissue defects, where the former presents stepwise errors, adapted, with permission from Ref. [179]. **e,** Flowchart for generating a conformal print path from scanned point cloud data. The point cloud data is first acquired, then expanded into a planar point cloud, and generate the planar zigzag path with preset parameters. The 2D path is recovered according to the z-axis coordinates to generate the 3D path, adapted, with permission from Ref. [179]. **f,** Projecting the 2D planar path onto the surface to be repaired, using the projection method to generate a surface conformal path, adapted, with permission from Ref. [180].

computational units such as logic decisions or machine-learning algorithms to correct errors and instabilities in the printing process [182–186]. In the inkjet-printing process, bioinks are dispensed in droplets, a one-dimensional forming unit, with controlled speed and volume to build 3D constructs. Wang et al. applied a voting-based law to compute the drive voltages in piezoelectric ink-jet printing based on images of droplet characteristics, including the numbers and areas of satellites [185]. The feedback was updated at a frequency of 5 Hz and presented effective printing correction under the external airstream disturbance. Bioink filament in extrusion-based bioprinting is another type of one-dimensional forming unit, and the nonuniformity in filament diameter due to inadequate or excessive extrusion will lead to printing defects within each printed layer. Jin et al. extracted spatially hierarchical features relying on CNNs from the 2D images of the printed structures and adjusted the material flow rate accordingly to compensate for the former deficiencies [187]. It is reported that the CNNs approach took 9 s from the defect detection to complete the correction, which is similar to the response time required for a human to identify the issues (Fig. 8a). Further, an investigation demonstrated the direct compensation for a two-dimensional plane through optical coherence tomography (OCT) scanning [172]. The OCT recognizes subtle changes in the morphology of the plane with coherent light diffraction and achieves a depth resolution below one μm. With the closed-loop feedback control, the average printing error was reduced to 5 μm in the

ink-jet bioprinting for 3D constructs (Fig. 8b). This feedback and compensation in two-dimensional resolves the errors that already occurred during one-dimensional traces bioprinting, but it also consumes much more time and hash-rate during the procedure.

The objects of *in vivo* bioprinting are dynamic biological systems, such as skin and soft organs in living bodies that undergo time-variant rigid transformations and non-rigid deformations induced by breathing, heartbeats, and surgical procedures. An online update of the printing toolpath is required to ensure high accuracy while *in situ* bioprinting on these dynamically deforming surfaces based on sensory data labeled adaptive bioprinting. O'Neill et al. were the first to validate the concept of adaptive bioprinting on a human hand with an XYZ gantry platform [188], where the distance between the printhead and the hand was computed via time of flight (TOF) based on the laser projector, and the relative location to the target was maintained in real-time. The gantry-based structure possesses a slow kinematic property that will result in an average printing error of 1.6 mm when the tracking target moves at 5 mm/s. Besides, this laser sensor only provides 3D translational tracking without compensating for 3D rotations. Whereas Zhu et al. implemented motion-tracking bioprinting with binocular vision as sensors and a parallel mechanism, Delta robot, as the actuator that presents improved kinematic response [124]. Benefits from this, the tracking error below 1.5 mm can be achieved for moving targets with speeds less than 42 mm/s by adjusting the motor speed in the
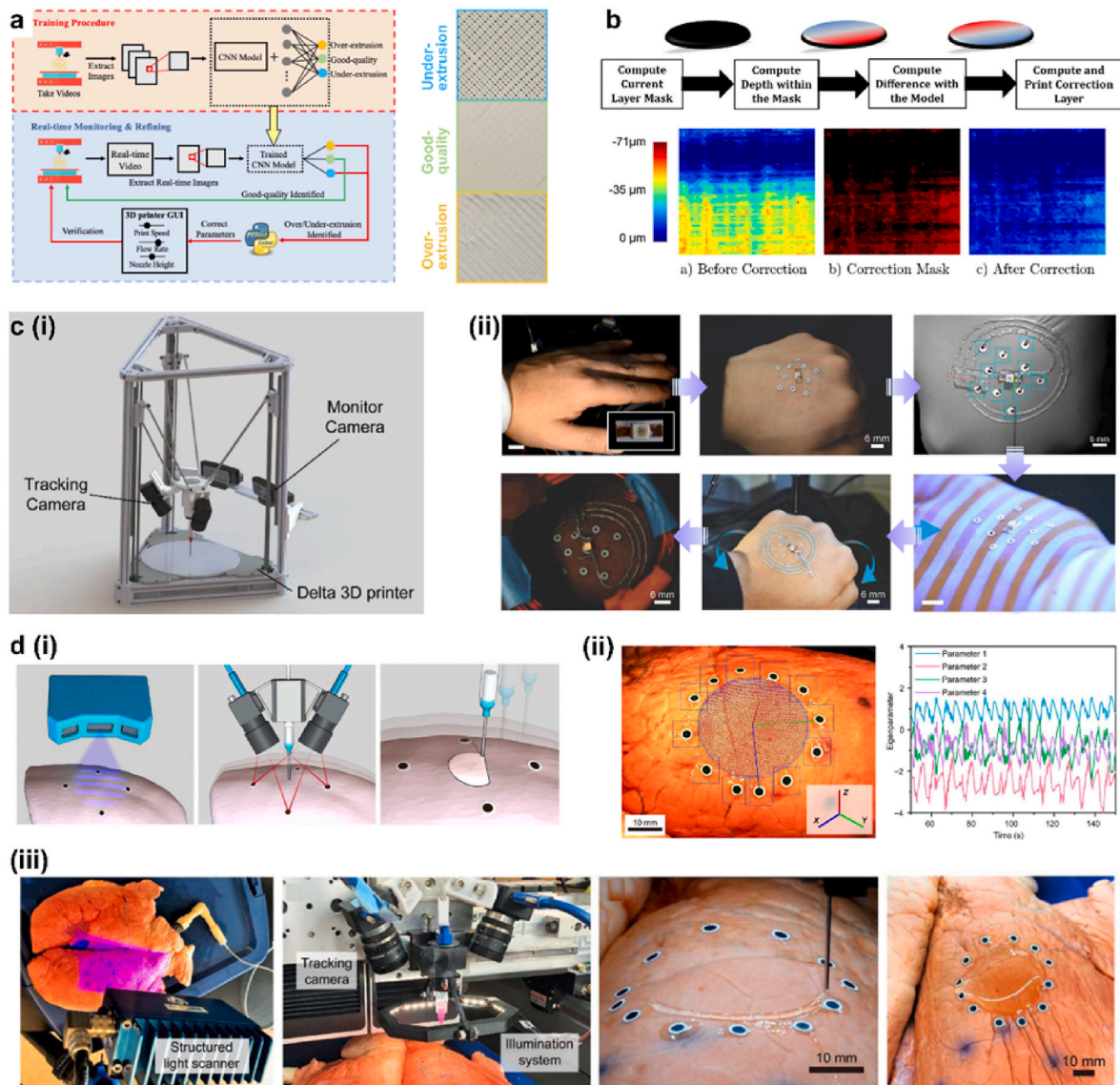
Fig. 8. a, Workflow of a closed-loop feedback-control algorithm based on CNN to adjust the diameter of the printed filament in real-time, adapted, with permission from Ref. [187]. **b,** Workflow of a layer-wise printing correction algorithm, with the current layer mask encoding the spatial information of where the material is expected to be placed in the current layer, adapted, with permission from Ref. [189]. **c,** Close-loop bioprinting system enables the printing process on moving freeform surfaces. (i) schematic diagram of the delta 3D printing robot with tracking camera. (ii) flowchart for printing high fidelity coils on a moving hand (Scale bars: 6 mm), adapted, with permission from Ref. [124]. **d,** 3D printed on a deformable porcine lung. (i) schematic diagram of the closed-loop bioprinting, where a model of the lung is first scanned, after which the spatial coordinates of the specific markers are acquired by a binocular vision to guide subsequent printing. (ii) the vision identifies specific points and the displacements of other unidentified points are acquired by interpolation (Scale bar: 10 mm). (iii) the stereovision guided gantry platform constructs a hydrogel layer *in situ* on a porcine lung (Scale bars: 10 mm), adapted from Ref. [116], CC BY 4.0.

mechanism. In addition, multiple markers were mounted near the target for sharp feature recognition and provided the tracking for 3D Euclidean motion (3D translation and rotation) (Fig. 8c). Furthermore, to address the limitations that the Delta mechanism has only three DoF and the challenges while printing on complicated surfaces, Zhao et al. integrated closed-loop control of the visual servo into the six-axis bioprinting robot, enabling the adaptive bioprinting in the six DoF level and addressing the deficiency of limited DoF [122].

Tracking the 3D Euclidean motion is insufficient for the accurate repair of tissues that undergo time-variant large deformations, such as a breathing lung or a beating heart. The computational speed of commonly used 3D perception methods, for instance, in a dense 3D point cloud, has difficulty reaching the pace of lung deformation and is further challenging for real-time tracking of such high-dimensional information. Zhu et al. proposed a "scan-inference" strategy to constitute a

closed-loop printing system, where a sequential 3D scanning of the target surface in static during the deformation was acquired, and only the fiducial markers were identified and located during the perception (Fig. 8d) [116]. For other unmarked surfaces, the deformations were calculated in an interpolation-inference approach, thus enabling real-time tracking and *in situ* bioprinting on the dynamically deforming surfaces. The average tracking error of 0.657 mm was demonstrated on a porcine breathing lung, further extending the applicability of *in vivo* bioprinting on dynamic biological systems.

2.3. Post-bioprinting stage

Theoretically, the integration with the surgical process approaches ends once the intraoperative implementation of bioprinting is complete. However, there still exist difficult points for in-depth exploration, for

instance, the review of the printing process that has occurred, as well as facilitating the attachment of the printed structures to the defects during the long-term postoperative stage for tissue regeneration.

The research presented above into the correction of the feedback system, by its very nature, is a hysteresis behavior, which is limited by the inherent latency in sensing, control, and computation. Failure to respond to the tissue deformation timely might result in a collision or penetration of the bioprinting devices into the tissues, affecting the printing quality and leading to tissue damage or safety issues. The movements of target surfaces and adjustments in the toolpath in multiple closed-loop bioprinting attempts can be utilized as a training dataset, from which the patterns of tissue deformation can be abstracted and predict the future states to constitute a feed-forward control and effectively address the above challenges and eliminate the potential risks. For interactivity, adaptability, and accuracy in predictive *in vivo* bioprinting, sophisticated machine learning algorithms and extensive training are required. Furthermore, this strategy is available for organs with quasi-repetitive deformations induced by lung movement during respiration etc., for which information containing time series can be targeted with gate recurrent unit (GRU) networks [190,191]. For unintended movements such as twitches, valid solutions are still lacking, and further exploration is necessary.

In terms of promoting post-operative tissue regeneration, the physiological regulation mechanisms for printed constructs can be established to align with their microenvironment, similar to a bioreactor. Dattatry et al. revealed the relationship between different loading parameters and the rate of bone regeneration through deep learning [192], and guided the rehabilitation of patients undergoing bone defects repair. Similar strategies have been applied to other tissue's post-operative recovery, including cardiac muscles [193,194] and skeletal muscles [195–197] etc., by exerting appropriate stimulation parameters, such as the amplitude and frequency of myoelectric excitation. These investigations assist in the physiological functional demonstration of printed tissue scaffolds and confer the *in vivo* bioprinting veritable feasibility in clinical application.

3. Conclusions and future perspectives

Since its introduction in 2007 for direct deposition of the bioinks into calvarial defects [126], *in vivo* bioprinting has received worldwide attention as an emerging therapeutic approach with potential clinical applications, with related studies showing a rapid upward trend according to Clarivate's report. In addition to its inherent advantages, such as using the body as a bioreactor and eliminating the risks associated with the manual implantation of pre-fabricated structures, this approach also broadens the range of available therapeutic techniques. To illustrate, the three categories of machining methods in the manufacturing industry, subtractive manufacturing, such as lathing and milling, equal-material manufacturing, such as casting and forging, and additive manufacturing, such as 3D printing, construct almost everything around us. In comparing medical procedures, the lesion's surgical removal can be likened to subtractive manufacturing, organ transplantation, and suturing to equal-material manufacturing, whereas additive manufacturing has no clinical treatment equivalent. *In vivo* bioprinting can be considered the therapeutic counterpart to additive manufacturing and might provide a treatment option for tissue deficiency diseases due to its personalized and "built-from-scratch" properties. For instance, with regard to injuries requiring personalized treatment, such as volumetric soft tissue loss caused by concussive blasts, *in vivo* bioprinting strategy is appropriate for arranging the printing process according to the location, morphology, and tissue types in the wound. Furthermore, with the ability to build out of nothing, this approach also offers advantages when dealing with sizeable internal tissue injuries like gastrointestinal perforation [119], where large structures that are hard to deliver into the body can be theoretically created intracorporeally through continuous delivery of bioink from outside the body. Thus, with these strengths conferred by the correspondence with additive manufacturing, this rising technology can address the challenges in tissue injury disease. Hopefully, *in vivo* bioprinting might compensate for the lack of tissue repair methods in current clinical protocols and serve the treatment of clinical diseases jointly with existing therapeutic strategies.

As the area of bioprinting develops and becomes ready for clinical application, the challenges and limitations of the novel strategy are becoming apparent. Primary in terms of the printing materials, i.e., bioinks, most efforts have focused on the modification and secondary development of the existing bioinks used in conventional bioprinting, but there is always a trade-off between the various properties of bioinks required for *in vivo* bioprinting. For the biomaterial components in bioinks, a specific design for the special *in vivo* physiochemical conditions is necessary to achieve better fidelity or integration of printed constructs to original tissues. For example, an investigation reported a strategy to enhance unilateral tissue adhesion using hydrinos migration in the stomach's acidic environment [198], but further exploration is necessary to adapt similar mechanisms to the more common internal environment with a neutral pH value. Among the challenges encountered in developing new synthetic materials that fulfill all the requirements above, tissue adhesion should be the primary insured property. The unique feature of *in vivo* bioprinting over conventional bioprinting is that the fabricated hydrogel structures cannot be sutured, which makes their attachment to the tissue dependent mainly on the adhesive properties. According to existing studies, faithful adherence to wounds is commonly met in conditions with dry surfaces, while challenges exist in wet or bleeding wounds. Consequently, when faced with significant blood loss injuries, like arterial hemorrhage, *in situ* wound closure through *in vivo* bioprinting is challenging. Pre-fabricated patches might be preferable for providing 6–8 times greater adhesive strength [98,100,199,200]. Research into the regulation of the printability and tissue adhesion of bioinks that serves *in vivo* bioprinting is currently being investigated [72,201]. Achieving more rapid formability and stronger tissue attachment might be a potential approach that addresses blood loss restrictions in wound healing.

A growing number of bioprinting strategies and bioinks currently allow for continuously improving resolutions, while faithfully reproducing the anatomy of the tissue does not ensure access to the functionality of the native tissue. Once finely controlled spatial deposition of cells and materials is achieved, biological constructs will undergo maturation and morphogenesis dominated by the cooperative function of multiple cells [202]. A few successful examples include *in vitro* fabricated ovaries with ovary follicle cells that were shown to rescue reproductive capacity [203], and printed spheroids of vascular and thyroid gland cells that were capable of replacing the bioactivity of native thyroid [204]. In addition, bioprinted muscle cell-laden hydrogel fibers demonstrated contractile functions after maturation into homogenous myofibers [205]. Although most of these studies were constructed *in vitro*, which circumvented the complex internal environment, these mechanistic explorations and breakthroughs will provide guidelines for the reconstruction of tissues. Another focus of bioink is the *in vitro* expansion of autologous cells to avoid unintended immune responses, which matters in the implementation of intracorporal bioprinting. A recent study demonstrated significant expansion for a wide range of stem cells through a special macropores scaffold that avoids the proliferative senescence and pluripotency loss common in laboratory expansion process [206], which might provide insight for bulk cell acquisition [207].

In parallel with bioinks, the modalities of *in vivo* bioprinting have scopes for further exploration. Taking the most progressive extrusion-based bioprinting approach as an example, UV-initiated photo-crosslinking is the mechanism with the most relevant applications. Despite its adaptability for internal or deeper tissue repair, these external cues might affect the surrounding healthy tissues, where the exact effects have not been comprehensively revealed. Currently, the photo-

crosslinking reactions induced by visible light [208,209] or NIR [61,62, 210,211] with less risk have been explored and, when combined with the extrusion-based bioprinting modality, might provide the benefits of both that provides safer internal tissue repair without affecting tissues nearby. In addition, given the robust scalability of the extrusion-based process, new composite bioprinting methods can be developed on its basis. For instance, unique hydrogel filaments in A-B heterogeneous or coaxial patterns have been constructed with the extrusion-based *in vivo* bioprinting approach [36], and further biological research has also been performed. An interesting study also presented a potential for incorporation with *in vivo* bioprinting. In order to improve the resolution in extrusion-based bioprinting, most efforts mainly focused on the optimization of printhead or materials' parameters. Differently, Santiago's group proposed the concept of continuous chaotic bioprinting that relied on the extrusion of chaotic advection to create microstructures at a resolution of less than 10 μm [212, 213]. With this strategy, a biomimetic muscle model that exhibited a hierarchical structure of highly aligned myotubes was printed, which might inspire the advances in repair for VML through *in vivo* bioprinting.

Replacing humans with mechanisms for productive labor should be the trend of future society, as their high accuracy and stability compensate for the errors in manual operation. As reported by Shugaba et al., robot-assisted surgery reduced the surgeons' musculoskeletal demands and released them from work-related injuries and related surgical instability [214]. Currently, robotics has been widely used in manufacturing, such as automobile production, and relevant technologies have developed. Yet there is still a lack of thorough investigations between robotics and *in vivo* bioprinting. On the one hand, bioprinting is a developing discipline, and few attentions have focused on transferring mature robotics to bioprinting. On the other hand, it is noteworthy that bioprinting works on living humans, which requires a high demand for intelligence. Current implements of bioprinting normally rely on time-consuming independent steps, including perception, reconstruction, toolpath planning, bioprinting, etc., and the integration of such processes with minimal human intervention has not been established yet. Artificial intelligence can perform, manage, and link these processes, represented by those closed-loop bioprinting research, and has been discussed in detail in a comprehensive review [189]. Undeniably, there is still a large between the realization of AI and current *in vivo* bioprinters due to the low error-tolerance in surgical procedures.

Advances in feedback systems, such as machine vision and inspection sensors, also improve robots' intelligence. In addition to the more efficient spatial localization algorithms described above for minimal latency, deformation modeling and prediction of target surfaces is another important topic, which enables the complete high-quality 3D reconstruction in the event of insufficient feature points and partial observability due to instrument occlusion or reflections. Combined with other sensors, such as joint torque sensors in the printing instruments for contact force detection, it is possible to achieve neurological-similar perception, including the comprehension of the semantic meaning of the 3D scene to distinguish instruments and tissues. These studies have reached a sophisticated stage at the theoretical level [215], but their application of them in real medical scenarios still needs effort.

There exists a transitional stage prior to the complete replacement of humans by robots, i.e., the development of human-controlled robot-assisted bioprinting systems. It integrates the advantages of handheld and automated devices to carry out the master-slave *in vivo* bioprinting, and has been demonstrated on several teleoperations performed on the da Vinci surgical system [216]. Overall, the *in vivo* bioprinting technique is becoming a reliable tool for the treatment of tissue injury diseases, and will exhibit its shining clinical value in the coming future.

Author's contributions

Wenxiang Zhao: Investigation, data curation, writing – original draft and visualization., **Chuxiong Hu:** Conceptualization, writing – review & editing, supervision, project administration, and funding acquisition., **Tao Xu:** Conceptualization, writing – review & editing, supervision.

Ethics approval and consent to participate

This is a review article and has no ethics approval and consent to participate to declare.

Declaration of competing interest

The authors declare no conflict of interest.

Acknowledgments

References

[1] M. Risbud, Tissue engineering: implications in the treatment of organ and tissue defects, Biogerontology 2 (2001) 117–125.

[2] F. Berthiaume, T.J. Maguire, M.L. Yarmush, Tissue engineering and regenerative medicine: history, progress, and challenges, Annual review of chemical and biomolecular engineering 2 (2011) 403–430.

[3] A. Gefen, K.J. Farid, I. Shaywitz, A review of deep tissue injury development, detection, and prevention: shear savvy, Ostomy/Wound Manag. 59 (2013) 26–35.

[4] D. Dindo, P.-A. Clavien, What is a surgical complication? World J. Surg. 32 (2008) 939–941.

[5] K.S. Lee, et al., The evolution of intracranial aneurysm treatment techniques and future directions, Neurosurg. Rev. (2021) 1–25.

[6] K. Thorsen, J.A. Søreide, J.T. Kvaløy, T. Glomsaker, K. Søreide, Epidemiology of perforated peptic ulcer: age-and gender-adjusted analysis of incidence and mortality, World J. Gastroenterol.: WJG 19 (2013) 347.

[7] P. Malfertheiner, F.K. Chan, K.E. McColl, Peptic ulcer disease, The lancet 374 (2009) 1449–1461.

[8] G. Karavani, et al., Endometrial thickness following early miscarriage in IVF patients–is there a preferred management approach? Reprod. Biol. Endocrinol. 19 (2021) 1–9.

[9] T.G. Weiser, et al., Estimate of the global volume of surgery in 2012: an assessment supporting improved health outcomes, Lancet 385 (2015) S11.

[10] O. Ljungqvist, M. Scott, K.C. Fearon, Enhanced recovery after surgery: a review, JAMA surg. 152 (2017) 292–298.

[11] A. Gawande, Two hundred years of surgery, N. Engl. J. Med. 366 (2012) 1716–1723.

[12] C. Dennis, et al., Suture materials—current and emerging trends, J. Biomed. Mater. Res. 104 (2016) 1544–1559.

[13] Nau-Hermes, M., Pollmanns, S. & Schmitt, R. in Key Engineering Materials. 317-326 (Trans Tech Publ).

[14] S.R. Maxwell, D.J. Webb, Improving medication safety: focus on prescribers and systems, Lancet 394 (2019) 283–285.

[15] J.K. Aronson, Medication errors: definitions and classification, Br. J. Clin. Pharmacol. 67 (2009) 599–604.

[16] S.V. Murphy, A. Atala, 3D bioprinting of tissues and organs, Nat. Biotechnol. 32 (2014) 773–785.

[17] C. Mandrycky, Z. Wang, K. Kim, D.-H. Kim, 3D bioprinting for engineering complex tissues, Biotechnol. Adv. 34 (2016) 422–434.

[18] P.S. Gungor-Ozkerim, I. Inci, Y.S. Zhang, A. Khademhosseini, M.R. Dokmeci, Bioinks for 3D bioprinting: an overview, Biomater. Sci. 6 (2018) 915–946.

[19] S. Vanaei, M. Parizi, F. Salemizadehparizi, H. Vanaei, An overview on materials and techniques in 3D bioprinting toward biomedical application, Eng. Regener. 2 (2021) 1–18.

[20] M. Wang, et al., The trend towards in vivo bioprinting, Int. J. Bioprint. 1 (2015).

[21] S. Singh, D. Choudhury, F. Yu, V. Mironov, M.W. Naing, In situ bioprinting–Bioprinting from benchside to bedside? Acta Biomater. 101 (2020) 14–25.

[22] M. Albanna, et al., In situ bioprinting of autologous skin cells accelerates wound healing of extensive excisional full-thickness wounds, Sci. Rep. 9 (2019) 1–15.

[23] O. Kérourédan, et al., In situ prevascularization designed by laser-assisted bioprinting: effect on bone regeneration, Biofabrication 11 (2019), 045002.

[24] D. Hakobyan, et al., *3D Bioprinting* 135-144, Springer, 2020.

[25] S. Duchi, et al., Handheld co-axial bioprinting: application to in situ surgical cartilage repair, Sci. Rep. 7 (2017) 1–12.

[26] S. Wüst, M.E. Godla, R. Müller, S. Hofmann, Tunable hydrogel composite with two-step processing in combination with innovative hardware upgrade for cell-based three-dimensional bioprinting, Acta Biomater. 10 (2014) 630–640.

[27] L. Ouyang, R. Yao, Y. Zhao, W. Sun, Effect of bioink properties on printability and cell viability for 3D bioplotting of embryonic stem cells, Biofabrication 8 (2016), 035020.

[28] Y. Zhao, et al., Three-dimensional printing of Hela cells for cervical tumor model in vitro, Biofabrication 6 (2014), 035001.

[29] K.C. Kolan, J.A. Semon, B. Bromet, D.E. Day, M.C. Leu, Bioprinting with human stem cell-laden alginate-gelatin bioink and bioactive glass for tissue engineering, Int. J. Bioprint. 5 (2019).

[30] M. Di Giuseppe, et al., Mechanical behaviour of alginate-gelatin hydrogels for 3D bioprinting, J. Mech. Behav. Biomed. Mater. 79 (2018) 150–157.

[31] N. Cao, X. Chen, D. Schreyer, Influence of calcium ions on cell survival and proliferation in the context of an alginate hydrogel, Int. Sch. Res. Notices (2012) 2012.

[32] Y.S. Zhang, et al., 3D extrusion bioprinting, Nat. Rev. Methods Prim. 1 (2021) 1–20.

[33] K.S. Lim, et al., Fundamentals and applications of photo-cross-linking in bioprinting, Chemical reviews 120 (2020) 10662–10694.

[34] Z. Zheng, et al., Visible light-induced 3D bioprinting technologies and corresponding bioink materials for tissue engineering: a review, Engineering 7 (2021) 966–978.

[35] A.I. Van Den Bulcke, et al., Structural and rheological properties of methacrylamide modified gelatin hydrogels, Biomacromolecules 1 (2000) 31–38.

[36] L. Ouyang, C.B. Highley, W. Sun, J.A. Burdick, A generalizable strategy for the 3D bioprinting of hydrogels from nonviscous photo-crosslinkable inks, Adv. Mater. 29 (2017), 1604983.

[37] K. Yue, et al., Synthesis, properties, and biomedical applications of gelatin methacryloyl (GelMA) hydrogels, Biomaterials 73 (2015) 254–271.

[38] D. O'Connell, C, et al., Development of the Biopen: a handheld device for surgical printing of adipose stem cells at a chondral wound site, Biofabrication 8 (2016), 015019.

[39] C.D. O'Connell, et al., Free-form co-axial bioprinting of a gelatin methacryloyl bio-ink by direct in situ photo-crosslinking during extrusion, Bioprinting 19 (2020), e00087.

[40] C. Di Bella, et al., In situ handheld three-dimensional bioprinting for cartilage regeneration, J. tissue eng. regener. med. 12 (2018) 611–621.

[41] K. Nuutila, et al., In vivo printing of growth factor-eluting adhesive scaffolds improves wound healing, Bioact. Mater. 8 (2022) 296–308.

[42] C.S. Russell, et al., In situ printing of adhesive hydrogel scaffolds for the treatment of skeletal muscle injuries, ACS Appl. Bio Mater. 3 (2020) 1568–1579.

[43] J.P. Quint, et al., In vivo printing of nanoenabled scaffolds for the treatment of skeletal muscle injuries, Adv. healthcare mater. 10 (2021), 2002152.

[44] A. Mostafavi, et al., Colloidal multiscale porous adhesive (bio) inks facilitate scaffold integration, Appl. Phys. Rev. 8 (2021), 041415.

[45] P. De la Puente, D. Ludeña, Cell culture in autologous fibrin scaffolds for applications in tissue engineering, Exp. Cell Res. 322 (2014) 1–11.

[46] H. Duong, B. Wu, B. Tawil, Modulation of 3D fibrin matrix stiffness by intrinsic fibrinogen–thrombin compositions and by extrinsic cellular activity, Tissue Eng. 15 (2009) 1865–1876.

[47] B.A. de Melo, et al., Strategies to use fibrinogen as bioink for 3D bioprinting fibrin-based soft and hard tissues, Acta Biomater. 117 (2020) 60–76.

[48] H. Gudapati, D. Parisi, R.H. Colby, I.T. Ozbolat, Rheological investigation of collagen, fibrinogen, and thrombin solutions for drop-on-demand 3D bioprinting, Soft Matter 16 (2020) 10506–10517.

[49] K. Laki, The polymerization of proteins: the action of thrombin on fibrinogen, Arch. Biochem. Biophys. 726 (2022), 109244.

[50] A.S. Wolberg, Thrombin generation and fibrin clot structure, Blood Rev. 21 (2007) 131–142.

[51] N. Hakimi, et al., Handheld skin printer: in situ formation of planar biomaterials and tissues, Lab Chip 18 (2018) 1440–1451.

[52] R.Y. Cheng, et al., Handheld instrument for wound-conformal delivery of skin precursor sheets improves healing in full-thickness burns, Biofabrication 12 (2020), 025002.

[53] J. Ku, et al., Cell-laden thermosensitive chitosan hydrogel bioinks for 3D bioprinting applications, Appl. Sci. 10 (2020) 2455.

[54] K.D. Roehm, S.V. Madihally, Bioprinted chitosan-gelatin thermosensitive hydrogels using an inexpensive 3D printer, Biofabrication 10 (2017), 015002.

[55] K.K. Moncal, et al., Controlled Co-delivery of pPDGF-B and pBMP-2 from intraoperatively bioprinted bone constructs improves the repair of calvarial defects in rats, Biomaterials 281 (2022), 121333.

[56] A. Mostafavi, et al., In situ printing of scaffolds for reconstruction of bone defects, Acta Biomater. 127 (2021) 313–326.

[57] M.H. Kim, S.Y. Nam, Assessment of coaxial printability for extrusion-based bioprinting of alginate-based tubular constructs, Bioprinting 20 (2020), e00092.

[58] J. Hazur, et al., Improving alginate printability for biofabrication: establishment of a universal and homogeneous pre-crosslinking technique, Biofabrication 12 (2020), 045004.

[59] C. Ash, M. Dubec, K. Donne, T. Bashford, Effect of wavelength and beam width on penetration in light-tissue interaction using computational methods, Laser Med. Sci. 32 (2017) 1909–1918.

[60] Lanzafame, R. Vol. 38 393-394 (Mary Ann Liebert, Inc., publishers 140 Huguenot Street, 3rd Floor New, 2020).

[61] Y. Chen, et al., Noninvasive in vivo 3D bioprinting, Sci. Adv. 6 (2020), eaba7406.

[62] A. Urciuolo, et al., Intravital three-dimensional bioprinting, Nat. biomed. eng. 4 (2020) 901–915.

[63] H. Gudapati, M. Dey, I. Ozbolat, A comprehensive review on droplet-based bioprinting: past, present and future, Biomaterials 102 (2016) 20–42.

[64] X. Li, et al., Inkjet bioprinting of biomaterials, Chem. Rev. 120 (2020) 10793–10833.

[65] C. Dou, et al., A state-of-the-art review of laser-assisted bioprinting and its future research trends, ChemBioEng. Rev. 8 (2021) 517–534.

[66] A. Skardal, et al., Bioprinted amniotic fluid-derived stem cells accelerate healing of large skin wounds, Stem cells transl. med. 1 (2012) 792–802.

[67] A. Skardal, et al., A tunable hydrogel system for long-term release of cell-secreted cytokines and bioprinted in situ wound cell delivery, J. Biomed. Mater. Res. B Appl. Biomater. 105 (2017) 1986–2000.

[68] V. Keriquel, et al., In situ printing of mesenchymal stromal cells, by laser-assisted bioprinting, for in vivo bone regeneration applications, Sci. Rep. 7 (2017) 1–10.

[69] V. Keriquel, et al., In vivo bioprinting for computer-and robotic-assisted medical intervention: preliminary study in mice, Biofabrication 2 (2010), 014101.

[70] K.K. Moncal, et al., Intra-operative bioprinting of hard, soft, and hard/soft composite tissues for craniomaxillofacial reconstruction, Adv. Funct. Mater. 31 (2021), 2010858.

[71] N. Hong, G.H. Yang, J. Lee, G. Kim, 3D bioprinting and its in vivo applications, J. Biomed. Mater. Res. B Appl. Biomater. 106 (2018) 444–459.

[72] A. Schwab, et al., Printability and shape fidelity of bioinks in 3D bioprinting, Chemical reviews 120 (2020) 11028–11055.

[73] S. Naghieh, X. Chen, Printability–A key issue in extrusion-based bioprinting, J. Pharm. Anal. 11 (2021) 564–579.

[74] J.R. Choi, K.W. Yong, J.Y. Choi, A.C. Cowie, Recent advances in photo-crosslinkable hydrogels for biomedical applications, Biotechniques 66 (2019) 40–53.

[75] M. Dovedytis, Z.J. Liu, S. Bartlett, Hyaluronic acid and its biomedical applications: a review, Eng. Regener. 1 (2020) 102–113.

[76] A. Chandrasekharan, et al., In situ photocrosslinkable hyaluronic acid-based surgical glue with tunable mechanical properties and high adhesive strength, J. Polym. Sci. Polym. Chem. 57 (2019) 522–530.

[77] S. Maiz-Fernández, A. Pérez-Álvarez, U. Silván, J.L. Vilas-Vilela, S. Lanceros-Mendez, Photocrosslinkable and self-healable hydrogels of chitosan and hyaluronic acid, Int. J. Biol. Macromol. 216 (2022) 291–302.

[78] R.H. Rakin, et al., Tunable metacrylated hyaluronic acid-based hybrid bioinks for stereolithography 3D bioprinting, Biofabrication 13 (2021), 044109.

[79] Y. Gao, X. Jin, Dual crosslinked methacrylated alginate hydrogel micron fibers and tissue constructs for cell biology, Mar. Drugs 17 (2019) 557.

[80] M. Hasany, et al., Synthesis, properties, and biomedical applications of alginate methacrylate (ALMA)-based hydrogels: current advances and challenges, Appl. Mater. Today 24 (2021), 101150.

[81] S. Jaiswal, P. Dutta, S. Kumar, J. Koh, S. Pandey, Methyl methacrylate modified chitosan: synthesis, characterization and application in drug and gene delivery, Carbohydr. Polym. 211 (2019) 109–117.

[82] C. Cui, W. Liu, Recent advances in wet adhesives: adhesion mechanism, design principle and applications, Prog. Polym. Sci. 116 (2021), 101388.

[83] H.Y. Yuen, H.P. Bei, X. Zhao, Underwater and wet adhesion strategies for hydrogels in biomedical applications, Chem. Eng. J. (2021), 133372.

[84] A. Chandra, T. Ruchti, V. Unnikrishnan, Computational modeling of wound suture: a review, IEEE Rev. Biomed. Eng. 11 (2018) 165–176.

[85] A.A. Adib, et al., Direct-write 3D printing and characterization of a GelMA-based biomaterial for intracorporeal tissue engineering, Biofabrication 12 (2020), 045006.

[86] L. Yu, et al., Microfluidic formation of core-shell alginate microparticles for protein encapsulation and controlled release, J. Colloid Interface Sci. 539 (2019) 497–503.

[87] S. Pradhan, J.M. Clary, D. Seliktar, E.A. Lipke, A three-dimensional spheroidal cancer model based on PEG-fibrinogen hydrogel microspheres, Biomaterials 115 (2017) 141–154.

[88] C. Beverly, R. Tanner, Numerical analysis of three-dimensional Bingham plastic flow, J. Non-Newtonian Fluid Mech. 42 (1992) 85–115.

[89] R.W. Ansley, T.N. Smith, Motion of spherical particles in a Bingham plastic, AIChE J. 13 (1967) 1193–1196.

[90] F. Li, et al., Cartilage tissue formation through assembly of microgels containing mesenchymal stem cells, Acta Biomater. 77 (2018) 48–62.

[91] Q. Feng, et al., Assembling microgels via dynamic cross-linking reaction improves printability, microporosity, tissue-adhesion, and self-healing of microgel bioink for extrusion bioprinting, ACS Appl. Mater. Interfaces 14 (2022) 15653–15666.

[92] M. Xie, et al., In situ 3D bioprinting with bioconcrete bioink, Nat. Commun. 13 (2022) 1–12.

[93] D. Ruiz-Molina, et al., Titel: the chemistry behind catechol-based adhesion the chemistry behind catechol-based adhesion, Angew. Chem. Int. Ed. Angew. Chem 10 (2018).

[94] M. Yu, T.J. Deming, Synthetic polypeptide mimics of marine adhesives, Macromolecules 31 (1998) 4739–4745.

[95] V. Ball, Polydopamine nanomaterials: recent advances in synthesis methods and applications, Front. Bioeng. Biotechnol. 6 (2018) 109.

[96] K. Huang, B.P. Lee, D.R. Ingram, P.B. Messersmith, Synthesis and characterization of self-assembling block copolymers containing bioadhesive end groups, Biomacromolecules 3 (2002) 397–406.

[97] C. Menzel, et al., Covalently binding mucoadhesive polymers: N-hydroxysuccinimide grafted polyacrylates, Eur. J. Pharm. Biopharm. 139 (2019) 161–167.

[98] H. Yuk, et al., Dry double-sided tape for adhesion of wet tissues and devices, Nature 575 (2019) 169–174.

[99] H. Yuk, et al., Rapid and coagulation-independent haemostatic sealing by a paste inspired by barnacle glue, Nat. biomed. eng. 5 (2021) 1131–1142.

[100] S.J. Wu, H. Yuk, J. Wu, C.S. Nabzdyk, X. Zhao, A multifunctional origami patch for minimally invasive tissue sealing, Adv. Mater. 33 (2021) 2007667.
[101] B.W. Walker, et al., Engineering a naturally-derived adhesive and conductive cardiopatch, Biomaterials 207 (2019) 89–101.
[102] D. Zhou, et al., Dopamine-modified hyaluronic acid hydrogel adhesives with fast-forming and high tissue adhesion, ACS Appl. Mater. Interfaces 12 (2020) 18225–18234.
[103] W. Zhang, et al., Catechol-functionalized hydrogels: biomimetic design, adhesion mechanism, and biomedical applications, Chem. Soc. Rev. 49 (2020) 433–464.
[104] D.W. Balkenende, S.M. Winkler, P.B. Messersmith, Marine-inspired polymers in medical adhesion, Eur. Polym. J. 116 (2019) 134–143.
[105] Q. Yang, et al., A bioinspired gallol-functionalized collagen as wet-tissue adhesive for biomedical applications, Chem. Eng. J. 417 (2021), 127962.
[106] Z. Tang, et al., Mussel-inspired cellulose-based adhesive with biocompatibility and strong mechanical strength via metal coordination, Int. J. Biol. Macromol. 144 (2020) 127–134.
[107] G. Ying, et al., An open-source handheld extruder loaded with pore-forming bioink for in situ wound dressing, Materials Today Bio 8 (2020), 100074.
[108] S.S. Das, et al., Laponite-based nanomaterials for biomedical applications: a review, Curr. Pharmaceut. Des. 25 (2019) 424–443.
[109] L. Li, et al., In situ repair of bone and cartilage defects using 3D scanning and 3D printing, Sci. Rep. 7 (2017) 1–12.
[110] L. Li, et al., Robotic in situ 3D bio-printing technology for repairing large segmental bone defects, J. Adv. Res. 30 (2021) 75–84.
[111] K. Ma, et al., Application of robotic-assisted in situ 3D printing in cartilage regeneration with HAMA hydrogel: an in vivo study, J. Adv. Res. 23 (2020) 123–132.
[112] W. Zhao, et al., Subaqueous bioprinting: a novel strategy for fetal membrane repair with 7-Axis robot-assisted minimally invasive surgery, Adv. Funct. Mater. 32 (2022), 2207496, https://doi.org/10.1002/adfm.202207496.
[113] B. Gatenholm, C. Lindahl, M. Brittberg, S. Simonsson, Collagen 2A type B induction after 3D bioprinting chondrocytes in situ into osteoarthritic chondral tibial lesion, Cartilage 13 (2021) 1755S–1769S.
[114] H. Ding, R.C. Chang, Simulating image-guided in situ bioprinting of a skin graft onto a phantom burn wound bed, Addit. Manuf. 22 (2018) 708–719.
[115] S.J. Joshi, R.M. Abed, Biodegradation of polyacrylamide and its derivatives, Environ. Proc. 4 (2017) 463–476.
[116] Z. Zhu, H.S. Park, M.C. McAlpine, 3D printed deformable sensors, Sci. Adv. 6 (2020) eaba5575.
[117] D.L. Cohen, J.I. Lipton, L.J. Bonassar, H. Lipson, Additive manufacturing for in situ repair of osteochondral defects, Biofabrication 2 (2010), 035004.
[118] J. Lipskas, K. Deep, W. Yao, Robotic-assisted 3D bio-printing for repairing bone and cartilage defects through a minimally invasive approach, Sci. Rep. 9 (2019) 1–9.
[119] W. Zhao, T. Xu, Preliminary engineering for in situ in vivo bioprinting: a novel micro bioprinting platform for in situ in vivo bioprinting at a gastric wound site, Biofabrication 12 (2020), 045020.
[120] S. Rauf, et al., Self-assembling tetrameric peptides allow in situ 3D bioprinting under physiological conditions, J. Mater. Chem. B 9 (2021) 1069–1081.
[121] T. Kean, M. Thanou, Biodegradation, biodistribution and toxicity of chitosan, Adv. Drug Deliv. Rev. 62 (2010) 3–11.
[122] W. Zhao, et al., Adaptive multi-degree-of-freedom in situ bioprinting robot for hair-follicle-inclusive skin repair: a preliminary study conducted in mice, Bioeng. Transl. Med. (2022), e10303.
[123] C. Zhou, et al., Ferromagnetic soft catheter robots for minimally invasive bioprinting, Nat. Commun. 12 (2021) 1–12.
[124] Z. Zhu, et al., 3D printed functional and biological materials on moving freeform surfaces, Adv. Mater. 30 (2018), 1707495.
[125] D.F. Duarte Campos, et al., Hand-held bioprinting for de novo vascular formation applicable to dental pulp regeneration, Connect. Tissue Res. 61 (2020) 205–215.
[126] P.G. Campbell, L.E. Weiss, Tissue engineering with the aid of inkjet printers, Expet Opin. Biol. Ther. 7 (2007) 1123–1127.
[127] X. Li, Q. Lian, D. Li, H. Xin, S. Jia, Development of a robotic arm based hydrogel additive manufacturing system for in-situ printing, Appl. Sci. 7 (2017) 73.
[128] K.M. Blevins, et al., In situ 3D bioprinting of musculoskeletal tissues in orthopedic surgery, J. 3D print. med. 6 (2022) 25–36.
[129] Z. Pazhouhnia, N. Beheshtizadeh, M.S. Namini, N. Lotfibakhshaiesh, Portable hand-held bioprinters promote in situ tissue regeneration, Bioeng. Transl. Med. (2022), e10307.
[130] H. Li, F. Cheng, D.P. Orgill, J. Yao, Y.S. Zhang, Handheld bioprinting strategies for in situ wound dressing, Essays Biochem. 65 (2021) 533–543.
[131] C.S. Russell, In Situ Bioprinting of Cell-Laden GelMA Scaffolds for the Treatment of Skeletal Muscle Defects, 2019.
[132] I.T. Ozbolat, K.K. Moncal, H. Gudapati, Evaluation of bioprinter technologies, Addit. Manuf. 13 (2017) 179–200.
[133] B. Tan, et al., Stereotactic technology for 3D bioprinting: from the perspective of robot mechanism, Biofabrication 13 (2021), 043001.
[134] L. Gao, et al., Research lab on 3D bioprinting of zhejiang university, Bio-Design and Manufact. 1 (2018) 211–214.
[135] H. Chen, et al., Robot-assisted in situ bioprinting of gelatin methacrylate hydrogels with stem cells induces hair follicle-inclusive skin regeneration, Biomed. Pharmacother. 158 (2023) 114140.
[136] P. Urhal, A. Weightman, C. Diver, P. Bartolo, Robot assisted additive manufacturing: a review, Robot. Comput. Integrated Manuf. 59 (2019) 335–345.
[137] P. Shakor, S. Nejadi, G. Paul, S. Malek, Review of emerging additive manufacturing technologies in 3D printing of cementitious materials in the construction industry, Front. Built Environ. 4 (2019) 85.
[138] T. Zhang, et al., IEEE 16th Conference on Industrial Electronics and Applications (ICIEA), 2021, pp. 1103–1108 (IEEE).
[139] C.H. Kuo, J.S. Dai, P. Dasgupta, Kinematic design considerations for minimally invasive surgical robots: an overview, Int. J. Med. Robot. Comput. Assist. Surg. 8 (2012) 127–145.
[140] N. Aghakhani, M. Geravand, N. Shahriari, M. Vendittelli, G. Oriolo, IEEE International Conference on Robotics and Automation, IEEE, 2013, pp. 5807–5812.
[141] R. Taylor, H. Paul, D. Khoramabadi, D. Larose, C. Cutting, Augmentation of human precision in computer-integrated surgery, Innov. technolo. biologie et médecine 13 (1992) 450–468.
[142] Kuo, C.-H. & Dai, J. S. in International Symposium on History of Machines and Mechanisms. 337-354 (Springer).
[143] F. Cepolina, R.P. Razzoli, An introductory review of robotically assisted surgical systems, Int. J. Med. Robot. Comput. Assist. Surg. 18 (2022), e2409.
[144] H. Sadeghian, F. Zokaei, S. Hadian Jazi, Constrained kinematic control in minimally invasive robotic surgery subject to remote center of motion constraint, J. Intell. Rob. Syst. 95 (2019) 901–913.
[145] H. Su, C. Yang, G. Ferrigno, E. De Momi, Improved human–robot collaborative control of redundant robot for teleoperated minimally invasive surgery, IEEE Rob. Autom. Lett. 4 (2019) 1447–1453.
[146] H. Su, et al., Toward teaching by demonstration for robot-assisted minimally invasive surgery, IEEE Trans. Autom. Sci. Eng. 18 (2021) 484–494.
[147] A.H. Khan, S. Li, X. Cao, Tracking control of redundant manipulator under active remote center-of-motion constraints: an RNN-based metaheuristic approach, Sci. China Inf. Sci. 64 (2021) 1–18.
[148] H. Su, et al., IEEE International Conference on Robotics and Automation (ICRA), 2020, pp. 4477–4482 (IEEE).
[149] T. Kastritsi, Z. Doulgeri, A controller to impose a RCM for hands-on robotic-assisted minimally invasive surgery, IEEE Trans. Med. Robot. Bionics 3 (2021) 392–401.
[150] H. Su, et al., IEEE/RSJ International Conference on Intelligent Robots and Systems (IROS), 2020, pp. 3151–3156 (IEEE).
[151] Z. Wang, W. Zhang, X. Ding, A Family of RCM mechanisms: type synthesis and kinematics analysis, Int. J. Mech. Sci. 231 (2022), 107590.
[152] F. Pugin, P. Bucher, P. Morel, History of robotic surgery: from AESOP® and ZEUS® to da Vinci, J. visceral surg. 148 (2011) e3–e8.
[153] O.M. Omisore, et al., A review on flexible robotic systems for minimally invasive surgery, IEEE Trans. Syst. Man, and Cybernet.: Systems 52 (2020) 631–644.
[154] R.J. Webster III, B.A. Jones, Design and kinematic modeling of constant curvature continuum robots: a review, Int. J. Robot Res. 29 (2010) 1661–1683.
[155] K. Jayaram, J. Shum, S. Castellanos, E.F. Helbling, R.J. Wood, IEEE International Conference on Robotics and Automation (ICRA), 2020, pp. 10305–10311 (IEEE).
[156] K.Y. Ma, P. Chirarattananon, S.B. Fuller, R.J. Wood, Controlled flight of a biologically inspired, insect-scale robot, Science 340 (2013) 603–607.
[157] C.D. Onal, R.J. Wood, D. Rus, An origami-inspired approach to worm robots, IEEE ASME Trans. Mechatron. 18 (2012) 430–438.
[158] H. Suzuki, R.J. Wood, Origami-inspired miniature manipulator for teleoperated microsurgery, Nat. Mach. Intell. 2 (2020) 437–446.
[159] D. Choudhury, S. Anand, M.W. Naing, The arrival of commercial bioprinters–Towards 3D bioprinting revolution, Int. J. Bioprint. 4 (2018).
[160] C.E. Garciamendez-Mijares, P. Agrawal, G. García Martínez, E. Cervantes Juarez, Y.S. Zhang, State-of-art affordable bioprinters: a guide for the DiY community, Appl. Phys. Rev. 8 (2021) 031312.
[161] M.A. Heinrich, et al., 3D bioprinting: from benches to translational applications, Small 15 (2019), 1805510.
[162] G. Savio, S. Rosso, R. Meneghello, G. Concheri, Geometric modeling of cellular materials for additive manufacturing in biomedical field: a review, Appl. Bionics Biomechanics (2018) 2018.
[163] S. Gómez, M. Vlad, J. López, E. Fernández, Design and properties of 3D scaffolds for bone tissue engineering, Acta Biomater. 42 (2016) 341–350.
[164] P. Abdollahiyan, F. Oroojalian, A. Mokhtarzadeh, M. de la Guardia, Hydrogel-based 3D bioprinting for bone and cartilage tissue engineering, Biotechnol. J. 15 (2020), 2000095.
[165] M. Singh, et al., 3D printed conformal microfluidics for isolation and profiling of biomarkers from whole organs, Lab Chip 17 (2017) 2561–2571.
[166] A. O'Riordan, T. Newe, G. Dooly, D. Toal, 12th International Conference on Sensing Technology (ICST), 2018, pp. 178–184 (IEEE).
[167] B. Tippetts, D.J. Lee, K. Lillywhite, J. Archibald, Review of stereo vision algorithms and their suitability for resource-limited systems, J. Real-Time Image Proc. 11 (2016) 5–25.
[168] A. Voulodimos, N. Doulamis, A. Doulamis, E. Protopapadakis, Deep Learning for Computer Vision: A Brief Review, in: Computational Intelligence and Neuroscience, 2018, p. 2018.
[169] J. Wu, Z. Jin, A. Liu, L. Yu, F. Yang, A survey of learning-Based control of robotic visual servoing systems, J. Franklin Inst. 359 (2022) 556–577.
[170] X. Sun, X. Zhu, P. Wang, H. Chen, IEEE 8th Annual International Conference on CYBER Technology in Automation, Control, and Intelligent Systems (CYBER), 2018, pp. 116–121 (IEEE).
[171] A.G. Stevens, et al., Conformal robotic stereolithography, 3D Print. Addit. Manuf. 3 (2016) 226–235.
[172] P. Sitthi-Amorn, et al., MultiFab: a machine vision assisted platform for multi-material 3D printing, ACM Trans. Graph. 34 (2015) 1–11.

[173] F. Liu, et al., Deep convolutional neural network and 3D deformable approach for tissue segmentation in musculoskeletal magnetic resonance imaging, Magn. Reson. Med. 79 (2018) 2379–2391.

[174] D.R. King, et al., Surgical wound debridement sequentially characterized in a porcine burn model with multispectral imaging, Burns 41 (2015) 1478–1487.

[175] J.E. Thatcher, et al., Imaging techniques for clinical burn assessment with a focus on multispectral imaging, Adv. Wound Care 5 (2016) 360–378.

[176] A. Holland, H. Martin, D. Cass, Laser Doppler imaging prediction of burn wound outcome in children, Burns 28 (2002) 11–17.

[177] R. Raizman, et al., Use of a bacterial fluorescence imaging device: wound measurement, bacterial detection and targeted debridement, J. Wound Care 28 (2019) 824–834.

[178] Q. Lian, et al., Path planning method based on discontinuous grid partition algorithm of point cloud for in situ printing, Rapid Prototyp. J. 25 (2019) 602–613.

[179] H. Wang, et al., Multi-tissue layering and path planning of in situ bioprinting for complex skin and soft tissue defects, Rapid Prototyp. J. 27 (2021) 321–332.

[180] G.M. Fortunato, et al., Robotic platform and path planning algorithm for in situ bioprinting, Bioprinting 22 (2021), e00139.

[181] G.M. Fortunato, E. Batoni, A.F. Bonatti, G. Vozzi, C. De Maria, Surface reconstruction and tissue recognition for robotic-based in situ bioprinting, Bioprinting 26 (2022), e00195.

[182] Lombardi III, J. P., Salary, R., Weerawarne, D. L., Rao, P. K. & Poliks, M. D. in International Manufacturing Science and Engineering Conference. V001T001A039 (American Society of Mechanical Engineers).

[183] G.P. Greeff, M. Schilling, Closed loop control of slippage during filament transport in molten material extrusion, Addit. Manuf. 14 (2017) 31–38.

[184] A. Saluja, J. Xie, K. Fayazbakhsh, A closed-loop in-process warping detection system for fused filament fabrication using convolutional neural networks, J. Manuf. Process. 58 (2020) 407–415.

[185] T. Wang, T.-H. Kwok, C. Zhou, S. Vader, In-situ droplet inspection and closed-loop control system using machine learning for liquid metal jet printing, J. Manuf. Syst. 47 (2018) 83–92.

[186] Y. Guo, J. Peters, T. Oomen, S. Mishra, IEEE International Conference on Advanced Intelligent Mechatronics (AIM), 2017, pp. 436–441 (IEEE).

[187] Z. Jin, Z. Zhang, G.X. Gu, Autonomous in-situ correction of fused deposition modeling printers using computer vision and deep learning, Manuf. Lett. 22 (2019) 11–15.

[188] J.J. O'Neill, R.A. Johnson, R.L. Dockter, T.M. Kowalewski, IEEE/RSJ International Conference on Intelligent Robots and Systems (IROS), 2017, pp. 934–940 (IEEE).

[189] Z. Zhu, D.W.H. Ng, H.S. Park, M.C. McAlpine, 3D-printed multifunctional materials enabled by artificial-intelligence-assisted fabrication technologies, Nat. Rev. Mater. 6 (2021) 27–47.

[190] R. Fu, Z. Zhang, L. Li, Youth Academic Annual Conference of Chinese Association of Automation (YAC), 2016, pp. 324–328 (IEEE).

[191] R. Dey, F.M. Salem, *IEEE 60th International Midwest Symposium on Circuits and Systems (MWSCAS)*. 1597-1600, IEEE, 2017.

[192] M. Dattatrey, A.K. Tiwari, B. Ghoshal, J. Singh, Predicting bone modeling parameters in response to mechanical loading, IEEE Access 7 (2019) 122561–122572.

[193] M.E. Kupfer, et al., In situ expansion, differentiation, and electromechanical coupling of human cardiac muscle in a 3D bioprinted, chambered organoid, Circ. Res. 127 (2020) 207–224.

[194] Mestre, R., Patiño, T., Guix, M., Barceló, X. & Sanchez, S. in Conference on Biomimetic and Biohybrid Systems. 205-215 (Springer).

[195] W. Kim, et al., A bioprinting process supplemented with in situ electrical stimulation directly induces significant myotube formation and myogenesis, Adv. Funct. Mater. 31 (2021), 2105170.

[196] Q. Yang, B. Gao, F. Xu, Recent advances in 4D bioprinting, Biotechnol. J. 15 (2020), 1900086.

[197] C. Paci, et al., Piezoelectric Nanocomposite Bioink and Ultrasound Stimulation Modulate Early Skeletal Myogenesis, Biomaterials Science, 2022.

[198] C. Cui, et al., A janus hydrogel wet adhesive for internal tissue repair and anti-postoperative adhesion, Adv. Funct. Mater. 30 (2020), 2005689.

[199] X. Kong, et al., An extensively adhesive patch with multiple physical interactions and chemical crosslinking as a wound dressing and strain sensor, ACS Appl. Polym. Mater. 4 (2022) 3926–3941.

[200] Y. Zhao, et al., Supramolecular adhesive hydrogels for tissue engineering applications, Chem. Rev. 122 (2022) 5604–5640.

[201] D. Chimene, R. Kaunas, A.K. Gaharwar, Hydrogel bioink reinforcement for additive manufacturing: a focused review of emerging strategies, Adv. Mater. 32 (2020), 1902026.

[202] J. Groll, et al., Biofabrication: reappraising the definition of an evolving field, Biofabrication 8 (2016), 013001.

[203] M.M. Laronda, et al., A bioprosthetic ovary created using 3D printed microporous scaffolds restores ovarian function in sterilized mice, Nat. Commun. 8 (2017) 1–10.

[204] E.A. Bulanova, et al., Bioprinting of a functional vascularized mouse thyroid gland construct, Biofabrication 9 (2017), 034105.

[205] M. Costantini, et al., Microfluidic-enhanced 3D bioprinting of aligned myoblast-laden hydrogels leads to functionally organized myofibers in vitro and in vivo, Biomaterials 131 (2017) 98–110.

[206] M.N.F.B. Hassan, et al., Large-scale expansion of human mesenchymal stem cells, Stem Cell. Int. 2020 (2020).

[207] L. Feng, et al., Three-dimensional printing of hydrogel scaffolds with hierarchical structure for scalable stem cell culture, ACS Biomater. Sci. Eng. 6 (2020) 2995–3004.

[208] I. Noshadi, et al., In vitro and in vivo analysis of visible light crosslinkable gelatin methacryloyl (GelMA) hydrogels, Biomater. Sci. 5 (2017) 2093–2105.

[209] H. Kumar, et al., Designing gelatin methacryloyl (GelMA)-Based bioinks for visible light stereolithographic 3D biofabrication, Macromol. Biosci. 21 (2021), 2000317.

[210] L.M. Stevens, C. Tagnon, Z.A. Page, Invisible" Digital Light Processing 3D Printing with Near Infrared Light, ACS Applied Materials & Interfaces, 2022.

[211] Y.J. Suh, et al., 3D printing and NIR fluorescence imaging techniques for the fabrication of implants, Materials 13 (2020) 4819.

[212] C.F. Ceballos-González, et al., High-throughput and continuous chaotic bioprinting of spatially controlled bacterial microcosms, ACS Biomater. Sci. Eng. 7 (2021) 2408–2419.

[213] E.J. Bolívar-Monsalve, et al., Continuous chaotic bioprinting of skeletal muscle-like constructs, Bioprinting 21 (2021), e00125.

[214] A. Shugaba, et al., Should all minimal access surgery Be robot-assisted? A systematic review into the musculoskeletal and cognitive demands of laparoscopic and robot-assisted laparoscopic surgery, J. Gastrointest. Surg. (2022) 1–11.

[215] A. Billard, D. Kragic, Trends and challenges in robot manipulation, Science 364 (2019), eaat8414.

[216] C. Freschi, et al., Technical review of the da Vinci surgical telemanipulator, Int. J. Med. Robot. Comput. Assist. Surg. 9 (2013) 396–406.